

# From ab Initio Potential Energy Surfaces to State-Resolved Reactivities: X + H<sub>2</sub>O $\leftrightarrow$ HX + OH [X = F, Cl, and O(<sup>3</sup>P)] Reactions

Jun Li,<sup>†,‡</sup> Bin Jiang,<sup>†</sup> Hongwei Song,<sup>†</sup> Jianyi Ma,<sup>§</sup> Bin Zhao,<sup>†</sup> Richard Dawes,<sup>||</sup> and Hua Guo\*,<sup>†</sup>

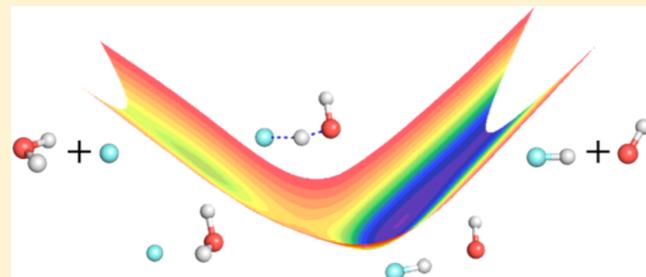
<sup>†</sup>Department of Chemistry and Chemical Biology, University of New Mexico, Albuquerque, New Mexico 87131, United States

<sup>‡</sup>School of Chemistry and Chemical Engineering, Chongqing University, Chongqing 400044, China

<sup>§</sup>Institute of Atomic and Molecular Physics, Sichuan University, Chengdu, Sichuan 610065, China

<sup>||</sup>Department of Chemistry, Missouri University of Science and Technology, Rolla, Missouri 65409, United States

**ABSTRACT:** We survey the recent advances in theoretical understanding of quantum state resolved dynamics, using the title reactions as examples. It is shown that the progress was made possible by major developments in two areas. First, an accurate analytical representation of many high-level ab initio points over a large configuration space can now be made with high fidelity and the necessary permutation symmetry. The resulting full-dimensional global potential energy surfaces enable dynamical calculations using either quasi-classical trajectory or more importantly quantum mechanical methods. The second advance is the development of accurate and efficient quantum dynamical methods, which are necessary for providing a reliable treatment of quantum effects in reaction dynamics such as tunneling, resonances, and zero-point energy. The powerful combination of the two advances has allowed us to achieve a quantitatively accurate characterization of the reaction dynamics, which unveiled rich dynamical features such as steric steering, strong mode specificity, and bond selectivity. The dependence of reactivity on reactant modes can be rationalized by the recently proposed sudden vector projection model, which attributes the mode specificity and bond selectivity to the coupling of reactant modes with the reaction coordinate at the relevant transition state. The deeper insights provided by these theoretical studies have advanced our understanding of reaction dynamics to a new level.



## I. INTRODUCTION

Chemical reactions are transformations of chemical species coupled with flows of energy in various forms, including vibrational, rotational, and relative translational energies. Kinetics describes the speed of reactions averaged over the relative kinetic energy and many reactant internal states. While rate coefficients provide useful information, however, a complete understanding of the reactivity of a gas phase bimolecular reaction is not possible without knowledge of its dependence on the collision energy and reactant internal state. The advent of the crossed molecular beam and laser techniques has revolutionized our ability to dissect dynamics of gas-phase and gas-surface reactions because they allow the precise control of the relative speed of the reactants and their internal states. These experiments have revealed a plethora of details of quantum state-resolved reaction dynamics.<sup>1–10</sup> Apart from the obvious dependence on the collision energy, ample evidence points to variance of the reactivity with reactant internal states.<sup>11,12</sup> This so-called mode specificity, and the related bond selectivity,<sup>13</sup> suggest that not all forms of energy are equal in promoting the reaction. As a result, a statistical treatment of the reaction dynamics, in which all forms of energy are considered as equals, may not be sufficient as dynamics often plays an important role.

The relative efficacy of the vibrational vs. translational excitation in the simplest activated atom–diatom reactions is

now well-understood.<sup>7,14,15</sup> Indeed, Polanyi has summarized a vast body of knowledge in two simple rules:<sup>16</sup> translational energy is more effective than vibrational energy in overcoming an “early” or reactant-like barrier, while the reverse is true for a “late” or product-like barrier. These intuitive and powerful rules have been instrumental in guiding our understanding of mode specificity in bimolecular reactions.<sup>11,12</sup> Nevertheless, Polanyi’s rules are difficult to extend to reactants beyond diatoms because the different vibrational modes are unlikely to have the same efficacy in promoting the reaction.<sup>17–19</sup> On the other hand, polyatomic reactions are often endowed with richer dynamics and surprising mode specificity, as discussed in more detail below.

Four-atom reactions provide an ideal proving ground for advancing our understanding of reaction dynamics and mode specificity. With more than one vibrational mode, these reactions allow the examination of the relative efficacy of the reactant vibrational modes among themselves and relative to the translational mode. The rotational degrees of freedom may also impact the reactivity differently. Hence, these systems are intrinsically more interesting than atom–diatom reactions.

**Received:** March 15, 2015

**Revised:** April 13, 2015

**Published:** April 17, 2015

Computationally, the treatment of six active degrees of freedom is well within the current capabilities of quantum dynamical algorithms.<sup>14,20</sup> Indeed, there are several recent examples of tetra-atomic reactive systems for which exquisite experimental observations have been accurately reproduced by first-principles quantum dynamics on accurate potential energy surfaces (PESs).<sup>21–24</sup> On the other hand, they are not as complex as reactions with even more atoms, which are much harder to treat quantum mechanically because of the larger number of degrees of freedom.<sup>25–27</sup> In this review, we focus on the hydrogen abstraction of water by various atomic radicals, including F, Cl, and O(<sup>3</sup>P), and their reverse reactions. Despite a common mechanism, the dynamics of the reactions is quite diverse. In Figure 1, it can be readily seen that these reactions possess rather

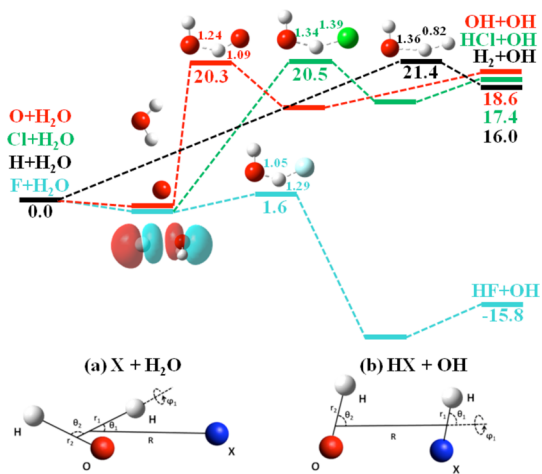


**Figure 1.** Top: schematic energetics (in kilocalories per mol relative to the respective reactant asymptotes) of the stationary points, including the reactant and product asymptotes, pre- and post-reaction complexes, and transition states, along the reaction paths of the four hydrogen abstraction reactions. The pre- and post-reaction wells are schematically shown without energies labeled. Note that the pre-reaction complexes F···H<sub>2</sub>O (with its singly occupied molecular orbital wave function shown) and Cl···H<sub>2</sub>O are hemibonded,<sup>175</sup> thus different from the pre-reaction complexes O···H<sub>2</sub>O and H···H<sub>2</sub>O. The forming and breaking bond distances (in Å) at the transition states are also shown. Note that the energies and geometries depend on the ab initio method (see text and references for further details). Bottom: the six-dimensional Jacobi coordinates for the X + H<sub>2</sub>O reactions in both the (a) atom-triatomic and (b) diatom–diatom forms.

different reaction energies and different locations of the reaction barriers. A systematic study of these systems provides valuable insights into important issues in reaction dynamics, such as transition-state control of reactivity, mode specificity, product energy disposal, tunneling, and stereodynamics. These reactions share some similarities with the H + H<sub>2</sub>O → H<sub>2</sub> + OH reaction, the mode specificity, and bond selectivity of which have been extensively studied.<sup>28–46</sup> For comparison, the energetics of this reaction is also included in the figure. Nevertheless, we note that the reactions discussed here are much more complex than the H + H<sub>2</sub>O reaction, which has neither significant pre- and post-reaction wells nor long-range interactions.<sup>47–51</sup>

There have been numerous experimental studies on the X + H<sub>2</sub>O ↔ HX + OH reactions, thanks to their importance in various gas phase environments such as atmospheres, interstellar media, and combustion. Apart from kinetic measurements, dynamical studies have revealed many interesting features on

mode specificity, bond selectivity, and product energy disposal. For the exoergic F + H<sub>2</sub>O reaction, for example, Setser and co-workers have observed strong vibrational excitation in the HF product.<sup>52,53</sup> Nesbitt and co-workers reported systematic crossed molecular beam studies of the F + H<sub>2</sub>O reaction and confirmed the inverted HF product vibrational state distribution.<sup>54</sup> In addition, these authors have reported ro-vibrational state distributions of the OH/OD coproduct of the F + H<sub>2</sub>O/D<sub>2</sub>O reactions and revealed that nonadiabatic transitions between the ground and first excited electronic states take place.<sup>55,56</sup> On the other hand, the Cl/O(<sup>3</sup>P) + H<sub>2</sub>O/HOD reactions have served as a prototype to understand the vibrational mode specificity and bond selectivity.<sup>57–59</sup> The dynamics of its reverse reaction HCl + OH has also been studied.<sup>60</sup> Finally, the O(<sup>3</sup>P) + H<sub>2</sub>O reaction has been investigated with the crossed molecular beam technique under hyperthermal conditions.<sup>61,62</sup> In addition to these bimolecular scattering experiments, photodetachment of negative ions XH<sub>2</sub>O<sup>-</sup> [X = F and O(<sup>3</sup>P)] has also been investigated by several authors,<sup>24,63–65</sup> which probes the neutral PESs near the transition states for the bimolecular reactions. These detailed dynamical experiments provided the backdrop for the theoretical studies discussed in this review.

We strive to provide a full-dimensional and accurate characterization of the dynamics of the title reactions necessary for a complete understanding of the mode specificity and bond selectivity. To this end, two important issues form the major stumbling blocks for a thorough understanding of the reaction dynamics. The first is the availability of accurate global PESs that govern the reaction dynamics. Until very recently, the existing PESs for these reactions had been either inaccurate, reduced dimensional, or limited in configuration space. These deficiencies prevented a quantitative description of the reaction dynamics. The second issue is the description of the reaction dynamics on a given PES. While the full-dimensional dynamics can be characterized with relative ease using the quasi-classical trajectory (QCT) method,<sup>66–68</sup> a quantitatively accurate description cannot be guaranteed without a quantum mechanical treatment because these hydrogen abstraction reactions may be strongly influenced by quantum effects such as zero-point energy, tunneling, and resonances. In what follows, we will discuss the tremendous progress in recent years in both the development of PESs and quantum dynamical (QD) characterization of the reaction dynamics. It is demonstrated that the convergence of the above two issues allowed the unraveling of fundamental principles governing reaction dynamics and endowed theory with predictive power.

## II. POTENTIAL ENERGY SURFACES

As discussed above, an inaccurate PES is not expected to yield correct results no matter how accurate the dynamical method might be. For four-atom reactions, indeed, the lack of accurate global PESs represented the main stumbling block in our understanding of reaction dynamics. We note that the direct dynamics method<sup>69</sup> requires no PES as the electronic energy is computed on the fly. However, this method can be very computationally expensive if a high-level ab initio method is used and is perhaps more importantly not easily amenable to quantum dynamical calculations due to the nonlocal nature of quantum mechanics. As a result, a first-principles understanding of reaction dynamics generally requires accurate global fitted PESs.

In this review, we limit our discussion to the adiabatic representation, in which a single electronic state is considered. Employing the Born–Oppenheimer (BO) approximation, the

electronic Schrödinger equation can be solved at particular nuclear geometries. The BO PES governing the nuclear motion is thus a representation of the electronic energy (plus nuclear repulsion energy) as a function of the molecular configuration. Today's ab initio electronic structure theory has advanced to a level that chemically accurate ( $\sim 1$  kcal/mol) energies can be routinely obtained for small molecular systems.<sup>70</sup> These calculations are often so efficient that one can afford to perform them on a large scale in order to map out the PES in the necessary configuration space relevant to the reaction under investigation. The key mathematical problem is thus becoming how to represent a vast number of ab initio points in a multidimensional space accurately and efficiently. For triatomic systems, such a representation can be achieved by brute-force cubic spline, as was done in some recent work.<sup>71,72</sup> However, spline methods become impractical for high-dimensional systems because of their low efficiency. Even in low dimensions, spline methods are generally not competitive with other methods in terms of accuracy, number of required points, and smooth behavior. The global PESs suitable for studying dynamics of polyatomic reactions such as those discussed here should satisfy the following conditions: (a) full-dimensional, including all internal degrees of freedom; (b) global, covering not only the strong interaction region, but also the reactant and product asymptotes; (c) invariant with respect to overall translation, rotation, and permutation of identical atoms in the system; (d) high fidelity in representing the ab initio points; (e) smooth and containing no discontinuities or artificial features; and (f) numerically efficient to evaluate.

There are two major strategies for fitting high-dimensional PESs. The first is based on global multivariate interpolation, which guarantees the PES to reproduce all ab initio data points. The reproducing kernel Hilbert space (RKHS)<sup>73</sup> and interpolating moving least-squares (IMLS) methods<sup>74–76</sup> both belong to this group. These methods can be quite accurate, capable of achieving subwavenumber convergence,<sup>75</sup> as long as sufficient points are used. However, multidimensional interpolation schemes can also become very expensive as the interpolation of each point requires a global calculation over the entire data set. One can improve the efficiency by interpolating locally.<sup>76</sup> Another good example of local interpolation is provided by the modified Shepard interpolation (MSI) method.<sup>77,78</sup> In this approach, the potential energy in the vicinity of an ab initio geometry is approximated with a second-order Taylor expansion in terms of the inverse internuclear distances. As a result, the PES passes through all the ab initio points in the data set. For an arbitrary geometry not in the data set, the potential energy is expressed as a distance-weighted sum of all nearby expansions within a confidence radius. With insufficient sampling, the local nature of the interpolation may make the PES quite bumpy. Even with the confidence radius, the MSI method can still be very time-consuming in multiple dimensions.

An alternative approach is to fit the ab initio points using global functions. These so-called "quasi-interpolation" approaches do not require the PES to pass through the ab initio points but attempt to minimize the global error of the fitting. The earliest functions used in representing PESs, such as the London-Eyring-Polanyi-Sato (LEPS), were physically inspired. Although they give a reasonable physical picture, their forms are often not sufficiently flexible to provide a faithful representation of the many ab initio points in a large configuration space. Many-body expansions in terms of polynomials of coordinates have long been used to represent PESs, as discussed by Murrell and

Varandas.<sup>79,80</sup> They are much more flexible than the earlier physically inspired forms and thus more successful for representing PESs. Similar approaches have been used by others.<sup>81–83</sup> To represent dissociation limits, it is more effective to use polynomials of inverted internuclear distances or exponential functions of these distances, as they level off when the molecule fragments. Bowman and co-workers have spearheaded the use of the permutation invariant polynomial (PIP) representation in which the PES is expanded in terms of symmetrized monomials:<sup>84</sup>

$$V = \sum_l c_l \hat{S} \prod_{i < j}^N p_{ij}^{l_{ij}} \quad (1)$$

where  $N$  is the number of atoms.  $p_{ij} = \exp(-\alpha r_{ij})$  are the Morse-like variables with  $\alpha$  as a length parameter and  $r_{ij}$  the  $N(N-1)/2$  internuclear distances.<sup>85</sup>  $l_{ij}$  is the degree of  $p_{ij}$ , and  $l = \sum_{i < j}^N l_{ij}$  is the total degree in each monomial.  $\hat{S}$  is the symmetrization operator which enforces the permutation symmetry in the system. The fitting is performed by a linear least-squares method, which is very efficient and robust. Thanks to the polynomial form, the evaluation of the PES is also quite inexpensive. This PIP approach has been widely used, including the systems discussed here, and the reader is referred to reviews on the details of the method and applications.<sup>85,86</sup>

An even more flexible global approach is based on neural networks (NNs). Here, an NN is essentially a nonlinear fitting tool that allows an accurate representation of a global PES.<sup>87</sup> In theory, it is capable of approximating any unknown real-valued multidimensional function up to arbitrary accuracy,<sup>88</sup> although errors are unavoidable in real applications. A typical feed-forward NN converts signals, namely, the input vector ( $\mathbf{G} = \{G_i\}$ ), to a scalar output [ $E$  (i.e., potential energy)] via one or more hidden layers of interconnecting neurons. The value of the  $k$ th neuron in the  $i$ th hidden layer can be written as,<sup>87</sup>

$$y_k^i = f_i(b_k^i + \sum_{j=1}^{N_{i-1}} w_{jk}^i y_j^{i-1}), \quad 1 \leq i \leq m \quad (2)$$

where  $N_{i-1}$  is the number of neurons in the  $(i-1)$ th layer;  $f_i$  are transfer functions for the  $i$ th layer;  $w_{jk}^i$  are weights that connect the  $j$ th neurons in the  $(i-1)$ th layer and the  $k$ th neurons in the  $i$ th layer, and  $b_k^i$  are the biases of the  $k$ th neurons of the  $i$ th layer, both of which act as an adjustable offset of the transfer functions. The output energy is expressed analogously as a single neuron in the  $(m+1)$  layer,

$$E = f_{m+1}(b_1^{m+1} + \sum_{j=1}^{N_m} w_{j1}^{m+1} y_j^m) \quad (3)$$

In most applications in PES fitting, it is rare to see NNs with more than two hidden layers. The parameters in the NN, such as the weights and biases, are determined by "training", using for example the Levenberg-Marquardt algorithm,<sup>89</sup> namely a nonlinear minimization of a performance function for the training set consisting of a large number of potential energy points in the relevant coordinate space. This performance function can be readily defined as the root-mean-square error (RMSE) of the fit:  $[(\sum_{i=1}^{N_{\text{data}}} (E_{\text{output}} - E_{\text{target}})^2) / N_{\text{data}}]^{1/2}$ , where  $E_{\text{target}}$  and  $E_{\text{output}}$  are the energy in the input and output, respectively. The implementation of the NN method is quite straightforward as easy-to-use and highly optimized NN software packages are available.<sup>90</sup>

In practice, the data set is often divided into the training, validating, and testing sets. To avoid false extrapolation due to edge points in the randomly selected validation and test sets, only fits with similar RMSEs for all three sets are accepted. In addition, the maximum deviation is also used in selecting the final NN PESs. The “early stopping” method is often used to avoid overfitting.<sup>87</sup> The final PES can be taken as an average of several best fits, as this so-called ensemble or committee approach further reduces the random error.<sup>91</sup> As discussed in several reviews<sup>88,92,93</sup> and a book,<sup>87</sup> recent applications of NNs in fitting PESs have demonstrated that they can often be more accurate and efficient than many alternatives.

For a molecular system, the PES is invariant under operations of the complete nuclear permutation and inversion (CNPI) group.<sup>79,85,88,94</sup> The inversion symmetry is automatically satisfied as the PES is a function of the internal coordinates or internuclear distances. The permutation symmetry, on the other hand, has to be enforced. To this end, one may impose the permutation symmetry by transforming a geometry to a symmetry-unique region before evaluating the PES.<sup>51,95</sup> This strategy, however, becomes impractical when a large number of permutation operations are required. Neither does it guarantee smooth behavior at the high-symmetry configurations, which are sometimes vital, such as the equilibrium geometry of CH<sub>4</sub>.<sup>96</sup> Alternatively, the permutation symmetry can be built intrinsically in the fitting function form, such as in the use of LEPS for simple triatomic systems or systematical PIPs for larger systems. In general, NNs do not automatically recognize permutation symmetry. The most primitive approach is to train the NN with a symmetrized data set by replicating data points in a symmetry-unique region to all other regions mandated by permutation.<sup>97–99</sup> However, the size of the set can be very large for molecules possessing large numbers of identical nuclei, and there is no guarantee that the symmetry is strictly preserved. A truly permutation symmetric PES can also be constructed by symmetrized neurons in the first hidden layer,<sup>100,101</sup> but it is system-dependent and has to involve modifications of the NN software in each case. We argue that the most effective approach to symmetry adaptation is to use symmetry functions of internuclear distances as the input of the NN.<sup>102–104</sup> To this end, we have recently proposed the PIP-NN method which uses the low-order PIPs as the symmetry functions in the NN fit of PESs.<sup>105,106</sup> The advantages of this PIP-NN approach are many-fold: it is rigorous, general, efficient, and simple to implement, as it combines the advantages of both the PIP and NN approaches for fitting PESs.

Taking the XH<sub>2</sub>O (X = F and Cl) systems as an example, the exchange of the two hydrogen nuclei should have no effect on the PES. Labeling the H, H, O, X as 1, 2, 3, 4, an intuitive choice of six PIPs to replace the six internuclear distances would be

$$G_1 = p_{12} \quad (4a)$$

$$G_2 = p_{34} \quad (4b)$$

$$G_3 = p_{13} + p_{23} \quad (4c)$$

$$G_4 = p_{14} + p_{24} \quad (4d)$$

$$G_5 = p_{13}p_{23} \quad (4e)$$

$$G_6 = p_{14}p_{24} \quad (4f)$$

where  $p_{ij}$  are defined in eq 1. Although these symmetry functions are indeed invariant with respect to the exchange  $(p_{13}, p_{14}) \leftrightarrow (p_{23}, p_{24})$ , which is the same as the identical nuclear permutation ( $1 \leftrightarrow 2$ ), as they should be, they are also invariant to bond interchanges:  $p_{14} \leftrightarrow p_{24}$  and/or  $p_{13} \leftrightarrow p_{23}$ , which implies the nonexistent permutation symmetries between  $r_{14}$  and  $r_{24}$  and/or between  $r_{13}$  and  $r_{23}$ . Consequently, the resulting form of the PES attempts to enforce the unphysical symmetry, leading to unacceptable errors in the fit. The solution to this problem is to include more PIPs, particularly cross term(s) such as

$$G_7 = p_{13}p_{14} + p_{23}p_{24} \quad (4g)$$

It is easy to verify that the term in eq 4g eliminates the false symmetries for the exchange of bond distances mentioned above. We note that this problem was first pointed out by Schmeltzer and Murrell almost 30 years ago.<sup>107</sup> They and subsequent authors<sup>85,108</sup> recognized that a permutation invariant PES requires not only the primary but also the secondary invariant polynomials.<sup>109</sup> For a system with  $M$  variables, there are  $M$  primary invariant polynomials which are algebraically independent. However, secondary invariants are also needed because they help to distinguish molecular configurations that have the same primary invariants. The number of secondary invariant polynomials is finite. In fact, the number and degrees of primary and secondary polynomial invariants can be determined using Molien's series<sup>110</sup> based on symmetry operations of the corresponding CNPI group.<sup>107,108</sup> For more discussion, the reader is referred to refs 85 and 106. In practice, our pragmatic approach to circumvent the problem is to include more PIPs than the number of internal coordinates. This poses no problem for numerical stability and efficiency of the NNs. We note in passing that gradients can be readily obtained analytically, although we have not yet implemented it.

The choice of the ab initio method used to generate the points for the global PES depends on the system. For some reactions, the coupled cluster method with singles, doubles, and perturbative triples [CCSD(T)] provides an accurate description of the PES. CCSD(T) is one of the most accurate post-Hartree–Fock electronic structure methods that in many cases captures a large fraction of the dynamic electron correlation energy.<sup>111</sup> It is also quite efficient for the X + H<sub>2</sub>O reactions discussed here. However, single-reference methods might not be appropriate for systems with a strong multireference nature, which can be probed by for example the T<sub>1</sub> diagnostic test.<sup>112</sup> Under such circumstances, multireference methods such as the configuration interaction (MRCI) method<sup>113</sup> are needed. We note that the recent emergence of the explicitly correlated methods has greatly improved the accuracy and efficiency of the ab initio calculations, as these F12/R12 methods have much faster convergence with respect to the size of the basis set.<sup>114</sup> In other words, the complete basis set limit can be approached with much smaller basis sets such as Dunning's aug-cc-pVTZ (AVTZ).<sup>115</sup> For some systems with important spin–orbit contributions, the spin–orbit coupling matrix elements or the corresponding corrections are computed at multiple configurations and fitted to analytical forms.<sup>116,117</sup>

The sampling of configuration space with ab initio points is an important issue if a globally accurate PES is to be constructed.<sup>86</sup> For a reactive PES, it is important to map out regions relevant to the reaction. Our strategy<sup>118,119</sup> is to first construct a primitive PES based on points sampled in the reaction valley, particularly near the stationary points and reaction path. Classical trajectories are then launched on the primitive PES to explore the

configuration space.<sup>77</sup> Additional points generated by the trajectories are screened against the existing points in the data set, using either an Euclidean<sup>87</sup> or generalized Euclidean criterion.<sup>120</sup> Those too close to the existing points in the data set are discarded. The ab initio energies of the new points are then generated and included in the fitting of the next PES. This process is iterated until all relevant configuration space is covered, and kinetic/dynamic results are converged. In our calculations, the low-energy points and those near the stationary points are often more heavily weighted to provide a better fit of those regions.

### III. REACTION DYNAMICS

As discussed above, the second challenge in theoretical reaction dynamics is the reactive scattering calculations on a PES. Ideally, reaction dynamics should be characterized by solving the nuclear Schrödinger equation with proper boundary conditions. This QD approach is of course the ultimate goal for understanding reaction dynamics. However, such QD calculations are often quite expensive, particularly at the state-to-state level, because of the exponential scaling with the number of coordinates in the system. In addition, the state-to-state QD calculations also suffer from the so-called “coordinate problem”, namely, the fact that no optimal coordinate system can be found for both the reactant and product channels. Currently, very few state-to-state QD studies have been reported for the title reactions using exact full-dimensional QD methods. New algorithms are being developed to circumvent these difficulties. In the mean time, there is often a need to treat the reaction dynamics approximately using the QCT method, which is significantly less expensive. QCT studies are also intuitive in providing mechanistic insights. However, the assumption that the nuclear motion is classical may lead to inaccurate and sometimes incorrect results stemming from the neglect of quantum effects such as zero-point energy, tunneling, and resonances, and ad hoc corrections are sometimes necessary. Below, we briefly discuss both the QCT and QD approaches.

**III.A. Quasi-Classical Trajectory Calculations.** The QCT approach is based on the premise that the nuclear motion on a BO PES can be approximated by Newtonian dynamics. This assumption is often reasonable as atoms are relatively heavy. From the quantum-classical correspondence principle, it is well-established that the QCT results are more reliable for heavy systems and at high temperatures. In addition, QCT is often quite accurate for highly averaged attributes such as total cross sections and rate coefficients. In a QCT calculation, the reactants are prepared semiclassically in specified ro-vibrational states.<sup>68</sup> This “quantization” of the reactant ro-vibrational modes gives rise to the term “quasi-classical”, as opposed to the pure classical approach. The trajectories are then propagated by solving the Newton’s equation numerically on the PES.

The product rotational angular momentum and vibrational energy can be quantized to yield information on the internal state distribution. Due to large energy gaps associated with vibrational energy levels, the quantization becomes particularly important. There are several methods to determine the vibrational energy and quantum numbers of molecular products.<sup>67,121</sup> The conventional way is to use a rectangular box centered at a quantum vibrational level and assign the trajectories in the box the corresponding vibrational quantum number.<sup>66</sup> This so-called histogram binning (HB) method is simple but has been shown to be sometimes inferior to an alternative binning method based on a Gaussian weighting function. In the Gaussian-binning (GB) method,<sup>122</sup> a narrow Gaussian centered at the quantum

vibrational level is used as a weighting function for each trajectory, and the final vibrational state distribution is a weighted sum of all trajectories. While often more reliable, the GB method requires a much larger number of trajectories to achieve statistical convergence.

**III.B. Quantum Dynamical Calculations.** For tetra-atomic reactions with heavy atoms, all QD calculations have been carried out using wave packet approaches. To study mode specificity, the total reaction ICS and its dependence on the reactant ro-vibrational excitation can be computed directly from the flux into the product channel. Such initial state specific wave packet (ISSWP) approach using the reactant Jacobi coordinates needs no coordinate transformation.<sup>123</sup> For the atom-triatom systems, for example, the Hamiltonian ( $\hbar = 1$ ) can be written in the A + BCD Jacobi coordinates (depicted in Figure 1) as<sup>123</sup>

$$\hat{H} = -\frac{1}{2\mu_R} \frac{\partial^2}{\partial R^2} + \hat{h}_1(r_1) + \hat{h}_2(r_2) + \frac{(\hat{j} - \hat{j}_{12})^2}{2\mu_R R^2} + \frac{\hat{l}_1^2}{2\mu_1 r_1^2} + \frac{\hat{j}_2^2}{2\mu_2 r_2^2} + \hat{V}(R, r_1, r_2, \theta_1, \theta_2, \varphi_1) - V_1^{\text{ref}}(r_1) - V_2^{\text{ref}}(r_2) \quad (5)$$

where  $R$  is the distance between A and the center of mass (COM) of BCD,  $r_1$  the distance between B and the COM of CD, and  $r_2$  the bond length of CD, with  $\mu_R$ ,  $\mu_1$ , and  $\mu_2$  as their corresponding reduced masses.  $\hat{j}_2$  is the rotational angular momentum operator of CD, and  $\hat{l}_1$  is the orbital angular momentum operator of atom B with respect to CD, which are coupled to form  $\hat{j}_{12}$ . The body-fixed (BF) frame is defined with the  $z'$  axis that coincides with  $R$  and  $r_1$  in the  $x'z'$  plane. The BF frame ( $x'y'z'$ ) is related to the space-fixed (SF) frame ( $xyz$ ) via a rotation defined by three Euler angles. The projections of the total angular momentum  $J$  onto the SF  $z$  axis and BF  $z'$  axis are given by  $M$  and  $K$ , respectively. We also define a molecular-fixed (MF) frame in which the  $z''$  axis lies along the  $r_1$  vector, and  $r_2$  is in the  $x''z''$  plane; the projection of the  $j_{12}$  onto the BF or MF frame is thus given by  $K$  or  $m$ , and  $m$  is also the projection of  $j_2$  onto the MF frame. The one-dimensional (1D) reference Hamiltonians are defined as

$$\hat{h}_i(r_i) = -\frac{1}{2\mu_i} \frac{\partial^2}{\partial r_i^2} + V^{\text{ref}}(r_i), \quad i = 1, 2 \quad (6)$$

where  $V^{\text{ref}}(r_i)$  are the corresponding 1D reference potentials along the coordinate  $r_i$ . A similar set of equations can be readily established for diatom–diatom reactions,<sup>123</sup> which are more conveniently described by the diatom–diatom Jacobi coordinates also depicted in Figure 1.

The parity ( $\epsilon$ ) adapted wave function is expanded as

$$\psi^{JMe}(\vec{R}, \vec{r}_1, \vec{r}_2) = \sum_{n, \nu_1, \nu_2, j, K} F_{n\nu_1\nu_2 j K}^{JMe} u_n^{\nu_1 \nu_2}(R) \phi_{\nu_1}(r_1) \phi_{\nu_2}(r_2) \times \Phi_{jK}^{JMe}(\hat{R}, \hat{r}_1, \hat{r}_2) \quad (7)$$

where  $n$  labels the translational basis functions,  $\nu_1$  and  $\nu_2$  denote the vibrational basis indices for  $r_1$  and  $r_2$ , and the composite index  $j$  represents  $(l_1, j_2$ , and  $j_{12})$ . The translational basis functions,  $u_n^{\nu_1}$ , depend on  $\nu_1$  due to the use of an L-shaped grid.<sup>124</sup> The parity-adapted coupled BF total angular momentum eigenfunctions,  $\Phi_{jK}^{JMe}(\hat{R}, \hat{r}_1, \hat{r}_2)$ , are defined as

$$\Phi_{jk}^{JMe} = (1 + \delta_{K0})^{-1/2} \sqrt{\frac{2J+1}{8\pi}} [D_{K,M}^{J*} Y_{l,j_2}^{j_{12}K} + \epsilon(-1)^{l_1+j_2+j_{12}+J} D_{-K,M}^{J*} Y_{l,j_2}^{j_{12}-K}] \quad (8)$$

where  $D_{K,M}^J$  are the Wigner rotation matrices<sup>125</sup> and  $Y_{l,j_2}^{j_{12}K}$  are defined as

$$Y_{l,j_2}^{j_{12}K} = \sum_m D_{Km}^{j_{12}*}(0, \theta_1, \varphi_1) \sqrt{\frac{2l_1+1}{4\pi}} \langle j_2 m l_1 0 | j_{12} m \rangle \times y_{j_2 m}(\theta_2, 0) \quad (9)$$

and  $y_{jm}$  denote the spherical harmonics. An alternative approach is to define the angular basis in the uncoupled form,<sup>126,127</sup> which depends on  $m$  instead of  $l_1$ ,

$$\Phi_{mj_2j_{12}K}^{JMe} = \sqrt{\frac{1}{(1 + \delta_{K0}\delta_{m0})}} \sqrt{\frac{2J+1}{8\pi}} [D_{K,M}^{J*} Y_{mj_2}^{j_{12}K} + \epsilon(-1)^J D_{-K,M}^{J*} Y_{mj_2}^{j_{12}-K}] \quad (10)$$

where  $Y_{mj_2}^{j_{12}K} = [(2j_{12}+1)/4\pi]^{1/2} D_{Km}^{j_{12}*}(0, \theta_1, \varphi_1) y_{j_2 m}(\theta_2, 0)$  and the uncoupled basis is thus related with the coupled one through a transformation,<sup>123</sup>  $Y_{l,j_2}^{j_{12}K} = \sum_m [(2l_1+1)/(2j_{12}+1)]^{1/2} \langle j_1 m l_1 0 | j_{12} m \rangle Y_{mj_2}^{j_{12}K}$ . Although the uncoupled basis is advantageous for transformation between a grid and basis representation when computing the action of the potential energy operator, the coupled one is more straightforward to truncate the basis size in  $j_{12}$  so as to achieve additional memory savings.

Two different propagators are often employed in our QD calculations: the split-operator propagator<sup>128</sup> and the real Chebyshev propagator.<sup>129</sup> As the former has been extensively discussed in the literature,<sup>123</sup> we focus here on our Chebyshev approach for tetra-atomic reactive systems.<sup>44,127,130,131</sup> In particular, the real initial wave packet  $|\chi_i\rangle$  is constructed as a direct product of a Gaussian wave packet in the scattering coordinate and a specific ro-vibrational state of BCD,  $|v_0 j_0 \tau; J\rangle$ ,

$$|\chi_i\rangle = N e^{-(R-R_0)^2/2\delta^2} \cos(k_i R) |v_0 j_0 \tau; J\rangle \quad (11)$$

where  $N$  is the normalization factor.  $R_0$  and  $\delta$  are the mean position and width of the initial Gaussian function and  $k_i$  is the mean momentum given by  $E_i$  via  $k_i = (2\mu_R E_i)^{1/2}$ .  $v_0$ ,  $j_0$ , and  $\tau$  denote the initial vibrational quantum number, the initial angular momentum quantum number, and the parity of the reactant BCD, respectively. The initial ro-vibrational wave function of the reactant BCD was obtained by diagonalizing its three-dimensional Hamiltonian. The initial wave packet can be constructed in either the SF or BF frame. In the SF frame, it is more convenient to calculate the scattering amplitude as it is directly related to the total orbital angular momentum, thus avoiding the long-range Coriolis term.<sup>132–134</sup> The initial wave packet in the SF frame is then converted to the BF frame before propagation. In the BF frame, the scattering amplitude can be approximately computed by backward propagating the initial Gaussian wave packet. The definition of the initial wave packet in the BF frame is preferred with the centrifugal sudden (CS, vide infra) approximation, where the Coriolis coupling is ignored.

The wave packet is then propagated using the Chebyshev propagator:<sup>135–137</sup>

$$|\psi_{k+1}\rangle = D(2\hat{H}_{\text{scaled}}|\psi_k\rangle - D|\psi_{k-1}\rangle), k \geq 1 \quad (12)$$

where  $|\psi_1\rangle = D\hat{H}_{\text{scaled}}|\psi_0\rangle$  and  $|\psi_0\rangle = |\chi_i\rangle$ . To impose outgoing boundary conditions, the following damping function  $D$  is applied at the grid edges:

$$D(\zeta) = e^{-a \left( \frac{\zeta - \zeta_a}{\zeta_{\max} - \zeta_a} \right)^n} \quad (13)$$

where  $\zeta = R$  and  $r_1$ , and  $\zeta_a$  is the starting point of the damping function. The scaled Hamiltonian is defined as  $\hat{H}_{\text{scaled}} = (\hat{H} - \bar{H})/\Delta H$  to avoid the divergence of the Chebyshev propagator outside the range  $[-1, 1]$ . The mean and half-width of the Hamiltonian are estimated from the spectral extrema  $H_{\min}$  and  $H_{\max}$  as  $\bar{H} = (H_{\max} + H_{\min})/2$  and  $\Delta H = (H_{\max} - H_{\min})/2$ . Since the initial wave packet is real, the Chebyshev propagation can be efficiently and accurately realized in real arithmetic,<sup>137</sup> which presents some numerical advantages. The Chebyshev propagation has been shown to be efficient and accurate, particularly for long propagations.<sup>138</sup>

The action of the Hamiltonian onto the Chebyshev wave packet is efficiently evaluated by transforming the wave function between the finite basis representation (FBR) and discrete variable representation (DVR).<sup>139</sup> The kinetic energy operator is diagonal in FBR except for the centrifugal potential term  $(\hat{J} - \hat{j}_{12})^2$ , which has a tridiagonal expression in the BF frame with the Coriolis coupling in off-diagonal positions. When the Coriolis coupling terms are included in the calculation, this dynamically exact approach is typically referred to as the close coupling or coupled channel (CC) method.<sup>123</sup> However, within the commonly used CS approximation,<sup>140,141</sup>  $(\hat{J} - \hat{j}_{12})^2$  is also diagonal,  $\langle \Phi_{jk}^{JMe} | (\hat{J} - \hat{j}_{12})^2 | \Phi_{jk}^{JMe} \rangle \approx \delta_{jj'} \delta_{KK'} [J(J+1) + j_{12} (j_{12} + 1) - 2K^2]$ , leading to significant savings for  $J > 0$ .

The flux through the dividing surface,  $S = [r_1 = r_1^F]$ , is calculated from the energy-dependent scattering wave functions, which are obtained by a cosine Fourier transform from the wave packet in the Chebyshev order domain at the dividing surface.<sup>142</sup> The initial state-selected total reaction probability is computed as follows:

$$P_{v_0 j_0 \tau K_0}^{J\epsilon}(E) = \frac{1}{2\pi\mu_1 |a_i(E)|^2 (\Delta H)^2 \sin^2 \theta} \times \text{Im} \left\langle \sum_k (2 - \delta_{k0}) e^{-ik\theta} \psi_k \right| \sum_{k'} (2 - \delta_{k'0}) e^{-ik'\theta} \left[ \delta(r_1 - r_1^F) \frac{\partial}{\partial r_1} \psi_{k'} \right] \right\rangle \quad (14)$$

where the Chebyshev angle  $\theta = \arccos E_{\text{scaled}}$  is a nonlinear mapping of the scaled energy with  $E_{\text{scaled}} = (E - \bar{H})/\Delta H$ . The energy amplitude of the initial wave packet at the collision energy  $E$  is given by  $a_i(E) = \langle \phi_{i\epsilon} | \chi_i \rangle$ , where  $|\phi_{i\epsilon}\rangle$  is the free scattering wave function.

The total reaction integral cross section (ICS) from a specific initial state is calculated by summing the reaction probabilities over all relevant partial waves:

$$\sigma_{v_0 j_0 \tau}(E) = \frac{1}{(2j_0 + 1)} \frac{\pi}{2\mu_R E} \sum_{K_0 \epsilon} \sum_{J \geq K_0} (2J+1) P_{v_0 j_0 \tau K_0}^{J\epsilon}(E) \quad (15)$$

The ICS can also be obtained using the  $J$ -shifting (JS) approximation,<sup>143</sup> in which the reaction probabilities for  $J > 0$  are computed by shifting the  $J = 0$  reaction probability:  $P^{J>0}(E) = P^{J=0}(E - \Delta E)$ , where  $\Delta E = B^* J(J+1)$  with  $B^*$  being the

rotational constant of the transition state. This JS approximation assumes the centrifugal term at the transition state lifts the barrier with increasing total angular momentum  $J$ , which is not a bad approximation for many activated reactions. This approximation can greatly reduce computational costs, but it may introduce large errors.

The QD state-to-state calculations for tetra-atom reactions are still quite challenging, and calculated cross sections have only been reported for the simplest  $\text{H} + \text{H}_2\text{O} \rightarrow \text{H}_2 + \text{OH}$  reaction.<sup>23,144,145</sup> As mentioned earlier, the major obstacle is the so-called “coordinate problem”, which requires a coordinate transformation when the wave packet is propagated from the reactant asymptote to product asymptote. One effective solution is based on the “reactant-product decoupling” (RPD) method,<sup>146–148</sup> which utilizes an absorbing potential in the product channel to capture the emerging wave packet in the reactant-based coordinates and propagate them using the product-based coordinates. However, it is not clear if this approach is still accurate when the product channel is dominated by a deep post-reaction well, as in the reactions discussed here.

Recently, a new way to calculate reactive S-matrix elements has been proposed by Manthe and co-workers,<sup>149</sup> which has been implemented by his group and ours for the accurate and efficient calculation of  $J=0$  state-to-state reaction probabilities<sup>150–153</sup> and cross sections.<sup>154</sup> In this approach, eigenstates of the thermal flux operator are first determined in the transition-state region and used as the initial transition-state wave packets (TSWP) for the propagations separately into both the reactant and product arrangement channels. This TSWP method is based on the quantum transition-state theory of Miller,<sup>155,156</sup> which provides a formulation for the direct calculation of the cumulative reaction probability (CRP) and thermal rate coefficient, using flux correlation functions. In the state-to-state version, the reactive S-matrix elements are assembled from the flux cross-correlation functions,<sup>149</sup>

$$S_{v_p \leftarrow v_r}(E) = \frac{e^{E/k_B T}}{2\pi\eta_{v_p}^{+*}(E)\eta_{v_r}^{-}(E)} \sum_n f_T^n A_{v_p \leftarrow n}(E) A_{n \leftarrow v_r}^*(E) \quad (16)$$

where the energy-specific projection amplitudes in the product ( $p$ ) and reactant ( $r$ ) channels are given as Fourier transforms of the corresponding flux cross-correlation functions:

$$\begin{aligned} A_{v_p \leftarrow n}(E) &= \int_{-\infty}^{\infty} dt e^{iEt} C_{v_p \leftarrow n}(t) \\ &= \int_{-\infty}^{\infty} dt e^{iEt} \langle \Phi_{v_p}^+ | e^{-i\hat{H}t} | f_T^n \rangle \end{aligned} \quad (17a)$$

$$\begin{aligned} A_{n \leftarrow v_r}^*(E) &= \int_{-\infty}^{\infty} dt e^{-iEt} C_{n \leftarrow v_r}^*(t) \\ &= \int_{-\infty}^{\infty} dt e^{-iEt} \langle f_T^n | e^{i\hat{H}t} | \Phi_{v_r}^- \rangle \end{aligned} \quad (17b)$$

Here  $\{f_T^n, |f_T^n\rangle\}$  are the thermal flux eigenpairs at the reference temperature of  $T$ ;<sup>157</sup> and  $\eta_{v_p}^+(E)$  and  $\eta_{v_r}^-(E)$  are energy normalizing factors of the asymptotic wave functions ( $|\Phi_{v_p}^+\rangle$  and  $|\Phi_{v_r}^-\rangle$ ) for the reactant and product channels, respectively. The latter are conveniently written as a Dirac delta function of the scattering coordinate multiplied by the reactant or product internal state wave functions.<sup>154</sup> Our own implementation relies on a mixed basis/grid representation using conventional time propagation,<sup>152,154</sup> which is different from the implementation of

Manthe and co-workers using the multiconfiguration time-dependent Hartree (MCTDH) propagation.<sup>149–151</sup>

In addition to its conceptual clarity, the TSWP method is also numerically efficient because it requires only “inelastic-type” calculations in each arrangement channels, thus greatly alleviating the “coordinate problem” in conventional reactive scattering calculations. In particular, the number of helicity channels, which often represents a bottleneck in state-to-state wave packet approaches to reactive scattering, is far fewer than what is needed in conventional calculations.<sup>154</sup> One of course has to transform the initial TSWPs into the appropriate Jacobi coordinates, but this transformation is done only once in a relatively small region near the transition state. In addition, the propagation of each TSWPs can be carried out independently in parallel to achieve high efficiency. Note that the entire S-matrix, rather than a column, is generated in such calculations at all energies. Furthermore, the inclusion of the Boltzmann factor makes the calculations numerically more stable and efficient by removing the singularity of the flux operator at the dividing surface and focusing on the low-energy eigenstates near the reaction barrier.<sup>158</sup> It has a further conceptual advantage, as it allows the analysis of the transition-state control of the state-to-state reaction dynamics.<sup>150</sup>

#### IV. SUDDEN VECTOR PROJECTION MODEL

As mentioned above, Polanyi’s rules are not readily extendable to reactions involving polyatomic reactants. To understand the mode specificity and bond selectivity in general, we have recently proposed a simple model.<sup>159–163</sup> This sudden vector projection (SVP) model is based on the premise that the collision time in an activated bimolecular reaction is typically much shorter than the time needed for energy randomization in the reactant channels before they form the transition state. In other words, the reaction can be considered to take place in the sudden limit. This is particularly true for molecules like  $\text{H}_2\text{O}$ , which has a sparse density of states and very slow rate for intramolecular vibrational energy redistribution (IVR).<sup>164</sup> In the sudden limit, the efficacy of a reactant mode, whether vibrational, rotational, or translational, in promoting the reaction is attributed to its coupling with the reaction coordinate at the transition state, which is approximated by the overlap between the reactant normal mode ( $\vec{Q}_i$ ) and the reaction coordinate vector ( $\vec{Q}_{RC}$ ):  $P_i = \vec{Q}_i \cdot \vec{Q}_{RC} \in [0,1]$ . The direction of the reaction coordinate is the same as that in the reaction-path Hamiltonian<sup>165</sup> at the transition state. Obviously, the larger the overlap, the higher the capacity for enhancing reactivity. By invoking microscopic reversibility, this SVP model can also be used to predict energy disposal in the products.<sup>159</sup> Like Polanyi’s rules, the SVP model emphasizes the importance of the transition state in controlling the mode specific reaction dynamics. However, our model emphasizes the coupling with the reaction coordinate at the transition state rather than the location of the barrier.

The implementation of the SVP model has been discussed in recent publications.<sup>159,160,163</sup> Unlike Polanyi’s rules, the SVP model is not restricted to atom–diatom reactions. Another distinct advantage is that the SVP model does not require a PES in order to make the predictions. Only the properties of the stationary points along the reaction pathway are needed.<sup>163,166</sup> As a result, it can be applied to large reactive systems, even where global PESs are not available, by direct ab initio calculations of the stationary point properties. This SVP model has been shown to be consistent with Polanyi’s rules for atom–diatom reactions, and it is amenable to reactions with polyatomic reactants. It has

**Table 1.** SVP Values for the  $X + H_2O \leftrightarrow HX + OH$  [ $X = H, F, Cl$ , and  $O(^3P)$ ],  $Cl + HOD \leftrightarrow HCl + OD$ , and  $Cl + DOH \leftrightarrow DCl + OH$  Reactions<sup>a</sup>

reaction	species	reactant side			product side		
		mode	SVP	species	mode	SVP	
$H + H_2O \leftrightarrow H_2 + OH$	$H + H_2O$	$H_2O$ symmetric stretch	0.66	$H_2 + OH$	$H_2$ vibration	0.37	
		$H_2O$ antisymmetric stretch	0.67		$H_2$ rotation	0.24	
		$H_2O$ bend	0.10		$OH$ vibration	0.01	
		$H_2O$ rotation I	0.04		$OH$ rotation	0.11	
		$H_2O$ rotation II	0.00		translation	0.89	
		translation	0.24				
$F + H_2O \leftrightarrow HF + OH$	$F + H_2O$	$H_2O$ symmetric stretch	0.30	$HF + OH$	$HF$ vibration	0.99	
		$H_2O$ antisymmetric stretch	0.28		$HF$ rotation	0.04	
		$H_2O$ Bend	0.12		$OH$ vibration	0.01	
		$H_2O$ rotation I	0.25		$OH$ rotation	0.05	
		$H_2O$ rotation II	0.83		translation	0.02	
		translation	0.25				
$Cl + H_2O \leftrightarrow HCl + OH$	$Cl + H_2O$	$H_2O$ symmetric stretch	0.71	$HCl + OH$	$HCl$ vibration	0.75	
		$H_2O$ antisymmetric stretch	0.70		$HCl$ rotation	0.50	
		$H_2O$ bend	0.07		$OH$ vibration	0.002	
		$H_2O$ rotation I	0.02		$OH$ rotation	0.05	
		$H_2O$ rotation II	0.03		translation	0.37	
		translation	0.05				
$O + H_2O \leftrightarrow OH + OH$	$O + H_2O$	$H_2O$ symmetric stretch	0.72	$OH + OH$	reactive $OH$ vibration	0.76	
		$H_2O$ antisymmetric stretch	0.69		reactive $OH$ rotation	0.58	
		$H_2O$ bend	0.04		$OH$ vibration	0.04	
		$H_2O$ rotation I	0.06		$OH$ rotation	0.16	
		$H_2O$ rotation II	0.00		translation	0.27	
		translation	0.05				
$Cl + HOD \leftrightarrow HCl + OD$	$Cl + HOD$	$OH$ stretch	0.99	$HCl + OD$	$HCl$ vibration	0.75	
		$OD$ stretch	0.09		$HCl$ rotation	0.25	
		$HOD$ bend	0.06		$OD$ vibration	0.01	
		$HOD$ rotation I	0.01		$OD$ rotation	0.09	
		$HOD$ rotation II	0.02		translation	0.21	
		translation	0.07				
$Cl + DOH \leftrightarrow DCl + OH$	$Cl + DOH$	$OH$ stretch	0.07	$DCl + OH$	$DCl$ vibration	0.73	
		$OD$ stretch	0.99		$DCl$ rotation	0.15	
		$HOD$ bend	0.05		$OH$ vibration	0.003	
		$HOD$ rotation I	0.05		$OH$ rotation	0.03	
		$HOD$ rotation II	0.04		translation	0.21	
		translation	0.08				

<sup>a</sup>See also refs 160, 183, 185, and 199.

been successfully applied to the title reactions, as well as many other gas phase and gas–surface reactions.<sup>167</sup> The predictions are in general reliable, although failures have been found.<sup>167</sup>

The success of this simple model attests to the important role of the transition state in controlling state-resolved reaction dynamics. Indeed, it is not difficult to see the spiritual similarity between the more qualitative SVP model and the quantitative TSWP method discussed in the previous section. In the discussion below, we will examine the predictive power of the SVP model for the title reactions. The SVP values for both the reactants and products of these reactions are listed in Table 1.<sup>160,162</sup> In addition, the SVP values for the  $Cl + HOD$  reactions are also presented in the same table for two nonequivalent transition states, to facilitate the discussion of the bond selective chemistry.

## V. REACTIVITY, MODE SPECIFICITY, BOND SELECTIVITY, AND PRODUCT ENERGY DISPOSAL

**V.A.  $F + H_2O \leftrightarrow HF + OH$ .** The existence of experimental state-to-state data makes this exoergic reaction very attractive for

QD studies. This reaction involves at least the three lowest-lying doublet electronic states. The lowest  $A'$  and  $A''$  states correlate adiabatically to both the reactants and products of the title reaction. While the excited  $A'$  state also correlates to the same reactants, it leads to  $HF(X^1\Sigma^+)$  and excited  $OH(A^2\Sigma^+)$  on the product side. Although the reaction pathway has been studied by several authors using high-level ab initio methods,<sup>168–172</sup> a full-dimensional global PES from the ground ( $\tilde{X}^2A'$ ) electronic state of the  $FH_2O$  system was not available until 2012, when Li, Dawes, and Guo (LDG) reported the first such PES.<sup>173</sup> These authors used the PIP method to fit more than 30000 points at the Davidson-corrected MRCI (MRCI+Q/AVTZ) level of theory with an RMSD error of  $294.1\text{ cm}^{-1}$ . In the LDG PES, the product side is augmented with an analytical potential to accurately account for the long-range dipole–dipole interaction between  $HF$  and  $OH$ .<sup>173</sup> Subsequently, the PES for the first excited electronic ( $\tilde{A}^2A''$ ) state was developed, and spin–orbit corrections were added to both PESs.<sup>174</sup>

The reaction pathway in the forward direction features a low barrier with a reactant-like transition state, flanked by relatively

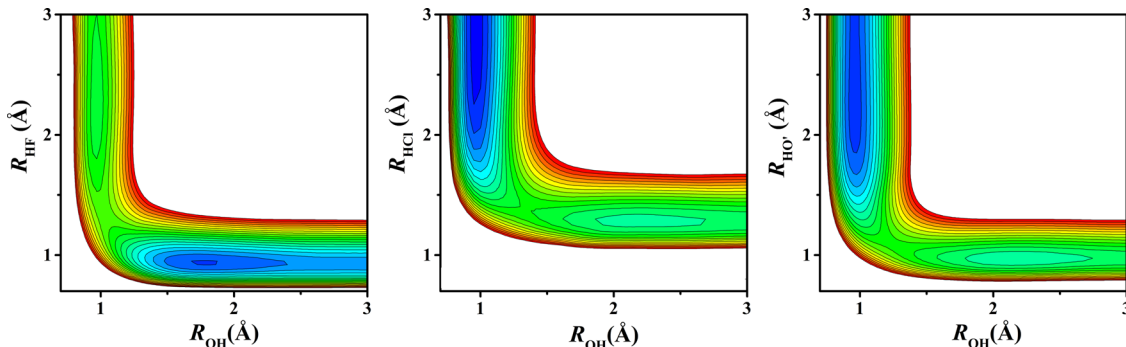


**Figure 2.** Potential energy surfaces for the  $\text{X} + \text{H}_2\text{O} \rightarrow \text{HX} + \text{OH}$  [ $\text{X} = \text{F}, \text{Cl}, \text{O}(^3\text{P})$ ] reactions along the reactive  $\text{X}-\text{H}$  and  $\text{O}-\text{H}$  distances when all other coordinates are relaxed.

deep pre- and a post-reaction wells, as illustrated in Figure 1. While the post-reaction complex is apparently due to a hydrogen bond between the HF and OH products, the pre-reaction  $\text{F}-\text{H}_2\text{O}$  complex was found to have a covalent nature, stemming from a three-electron two-center hemibond between the F radical and a lone electron pair of the water oxygen.<sup>175</sup> This covalent complex, which is quite strong with a binding energy of 2.21 kcal/mol with the spin-orbit correction, has an interesting geometry as shown in Figure 1. As discussed below, it has a significant influence on the reaction dynamics, particularly at low-collision energies. After the spin-orbit correction, the barrier heights for the ground and first excited electronic states are 4.20 and 17.57 kcal/mol, respectively. The barrier height in the ground state was later revised downward to 1.92–2.30 kcal/mol based on higher-level calculations,<sup>170,171,173,176</sup> which could better capture the higher-order electron correlation. This progression of changes underscores the importance of electron correlation in reaction dynamics. The entire PES was adjusted accordingly using an external scaling method.<sup>176</sup> It has been shown that the scaled PES is capable of reproducing the measured rate coefficients and kinetic isotope effect for the forward reaction,<sup>176</sup> as well as the experimental absolute total cross section.<sup>177</sup> More recently, the LDG PES has been refitted using the PIP-NN method, which lowered the RMSE to 54.8 cm<sup>-1</sup>.<sup>106</sup> In Figure 2, the PES is depicted along the F–H and O–H distances.

The QCT method was used to compute the reaction cross sections on the LDG PES, neglecting nonadiabatic transitions. It was found that the reactivity in the forward direction is significantly enhanced at low-collision energies, stemming apparently from the pre-reaction complex between F and  $\text{H}_2\text{O}$ .<sup>178</sup> The geometry of this complex, shown in Figure 1, is such that the incoming trajectories are strongly influenced by the stereodynamical forces, which steer them toward the transition state. The conclusion that the pre-reaction complex can enhance the reactivity is verified by QD calculations of  $J = 0$  reaction probabilities.<sup>178</sup> In addition, more recent QD calculations found sharp peaks in the reaction probabilities, which can be attributed to tunneling resonances supported by the relatively deep pre-reaction well and low barrier on the PES.<sup>153</sup> The stereodynamics bears some similarity with several previously identified cases where pre-reaction complexes strongly influence the outcome of the bimolecular reactions.<sup>179–181</sup>

Even more interestingly, both QCT and QD (CS) calculations on the LDG PES revealed that the forward reactivity is significantly enhanced by the excitation of  $\text{H}_2\text{O}$  vibrations.<sup>182</sup> In fact, the excitation of all three vibrational modes was found to

enhance the reaction more effectively than translational excitation, except for at very low translational energies (as shown in Figure 3). This is quite surprising as this reaction has a

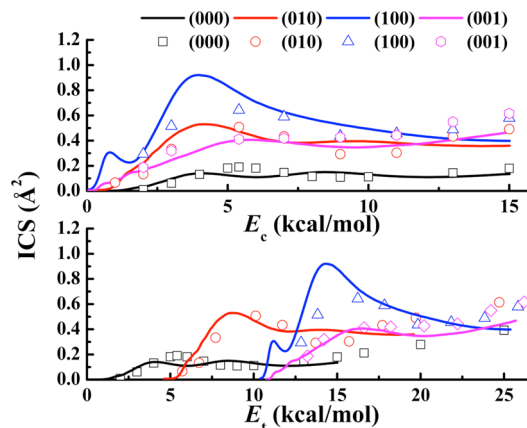


**Figure 3.** ICSs for the  $\text{F} + \text{H}_2\text{O}(n_1, n_2, n_3) \rightarrow \text{HF} + \text{OH}$  reaction with various  $\text{H}_2\text{O}$  vibrational states obtained from both QCT (symbols) and QD (lines) calculations. These excitation functions are plotted in collision energy (top) and total energy (bottom). The latter is referenced to the ro-vibrational ground state, namely,  $\text{F} + \text{H}_2\text{O}(0,0,0)$ . Adapted from ref 182. Copyright 2013 American Chemical Society.

decidedly early barrier. With a naive extension of Polanyi's rules, translational energy would be more effective in promoting such a reaction than any vibrational excitation of the  $\text{H}_2\text{O}$  reactant. The failure of the extended Polanyi's rules in predicting the mode specificity in this reaction clearly suggests the need to find more general rules of thumb. The SVP model, which is not based on the location of the barrier, successfully explained the observed mode specificity.<sup>160</sup> In particular, the enhancement effects of the three vibrational modes of  $\text{H}_2\text{O}$  can be attributed to their relatively strong couplings with the reaction coordinate at the transition state, as shown in Table 1, despite the fact that the transition state resembles the reactants. Interestingly, the SVP model also predicted a strong promotional effect for the reactant rotational excitation,<sup>162</sup> which was later confirmed by both QCT and QD CS calculations.<sup>153,162,177</sup>

QCT calculations on the LDG PES revealed strong vibrational excitation and moderate rotational excitation in the HF product, while the OH product was found to be internally cold.<sup>173,174,177</sup> The inverted HF vibrational state distribution, almost independent of the binning method, is consistent with the experimental findings.<sup>54</sup> In addition, the measured rotational state distributions of the products HF and OH are also

reproduced well by the QCT method. Very recently, quantum TSWP calculations with zero total angular momentum also confirmed the inverted HF vibrational state distribution and the relatively cold rotational distributions for both products<sup>153</sup> (as shown in Figure 4). These product state distributions are

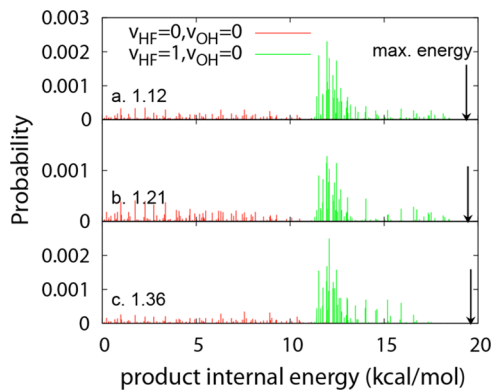


**Figure 4.** Final product internal state distributions for the  $\text{F} + \text{H}_2\text{O}(0,0,0, J_{\text{K},\text{K}}) \rightarrow \text{HF} + \text{OH}$  reaction at three collision energies: (a) 1.12 kcal/mol, (b) 1.21 kcal/mol, and (c) 1.36 kcal/mol, calculated using a QD method with  $J = 0$ . The product ro-vibrational energy is measured relative to the sum of the ground ro-vibrational energies of HF and OH. The maximal allowed energy is indicated in the figure by arrows. Adapted from ref 153. Copyright 2015 American Chemical Society.

consistent with the SVP values in Table 1, which predict that the H–F vibration is strongly coupled with the reaction coordinate at the transition state, while other product modes are almost orthogonal to the reaction coordinate. In addition, the QCT

calculated differential cross section is largely backward, suggesting a direct rebound mechanism.<sup>173</sup>

The PESs of the two lowest electronic states of this system were recently used to simulate the photodetachment of  $\text{FH}_2\text{O}^-$ .<sup>24</sup> The stable anion has an equilibrium geometry resembling the transition state of the neutral reaction. In the Condon approximation, the anion wave function is placed vertically on the neutral PESs of both the ground and first excited electronic states when the electron is ejected (as depicted in Figure 5). These wave packets subsequently dissociate toward both the reactant and product asymptotes of the  $\text{F} + \text{H}_2\text{O} \leftrightarrow \text{HF} + \text{OH}$  reaction. Our full-dimensional quantum dynamical model of the photodetachment revealed that the ground electronic state plays a dominant role at the experimental photon frequency, and the dissociation prefers the HF + OH asymptote.<sup>24</sup> Like the bimolecular reaction, the photodetachment of  $\text{FH}_2\text{O}^-$  also leads to a strong HF vibrational excitation. In addition to reproducing the experimental photoelectron-photofragment coincidence spectrum, our calculations also revealed the important role played by Feshbach resonances supported by the deep post-reaction well in the dissociation dynamics. Evidence for these long-lived metastable states was found in the experiment.<sup>24</sup>

The aforementioned salient dynamical features persisted on the new and more accurate PIP-NN PES.<sup>106</sup> This PIP-NN PES was recently employed to investigate the mode specificity of the reverse  $\text{HF} + \text{OH} \rightarrow \text{F} + \text{H}_2\text{O}$  reaction using QCT and QD methods with and without the CS approximation. Consistent with the prediction of the SVP model, it was found that the HF vibration strongly promotes the reaction, while the OH vibration has essentially no effect (as shown in Figure 6). On the other hand, rotational excitation of each diatomic reactant slightly enhances the reactivity.<sup>183</sup> These behaviors can be readily understood in terms of microscopic reversibility and are

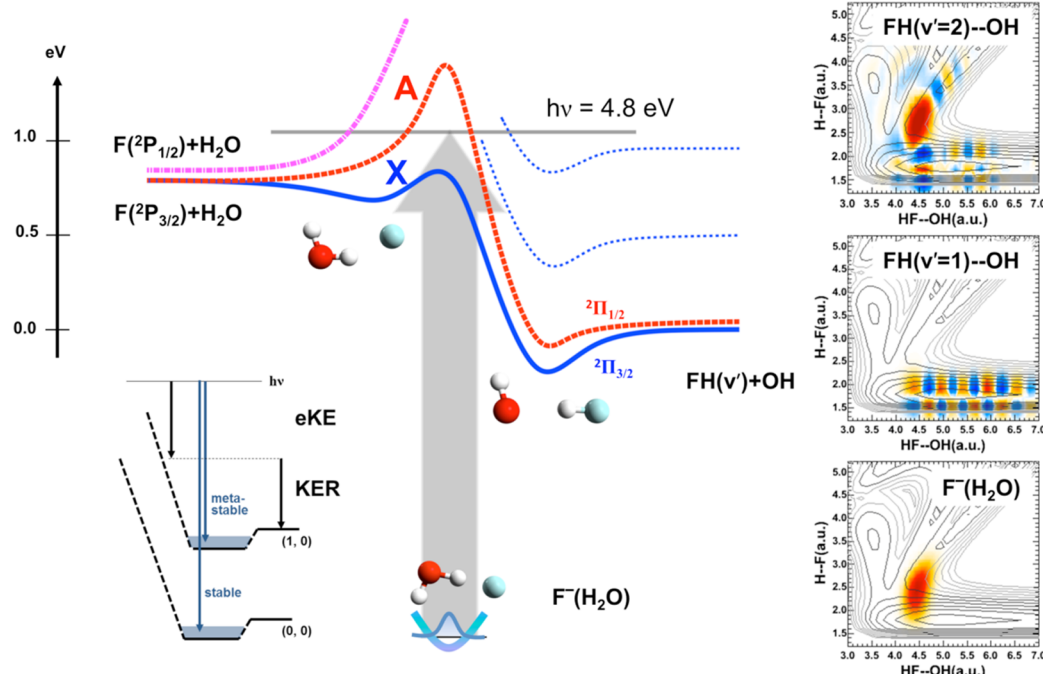


**Figure 5.** Illustration of the photodetachment experiment: the  $\text{F}^-(\text{H}_2\text{O})$  anion is projected onto the two lowest electronic states of the neutral species [i.e., the ground ( $X$ ) and the excited ( $A$ ) states], followed by fragmentation into both the  $\text{F} + \text{H}_2\text{O}$  and  $\text{HF} + \text{OH}$  channels. The scattering functions in the right panels indicate strong Feshbach resonances in the product channel. Adapted with permission from ref 24. Copyright 2014 American Association for the Advancement of Science.

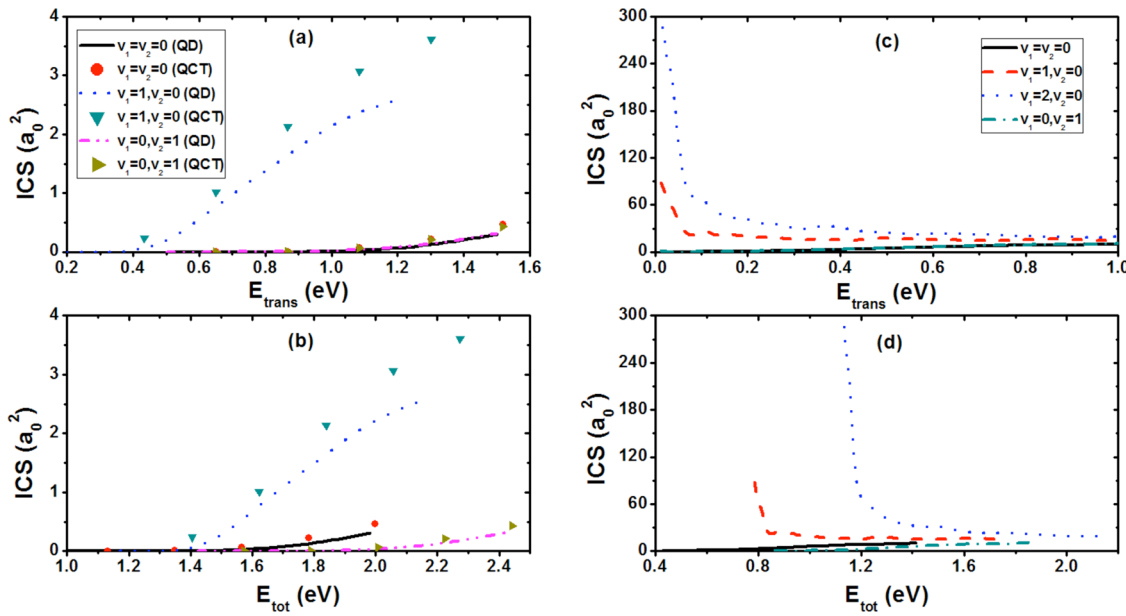


**Figure 6.** QD and QCT ICSs for the  $\text{HF}(\nu_1 = 0, 1; j_1 = 0) + \text{OH}(\nu_2 = 0, 1; j_2 = 0) \rightarrow \text{F} + \text{H}_2\text{O}$  reaction and QD ICSs for the  $\text{HCl}(\nu_1 = 0-2; j_1 = 0) + \text{OH}(\nu_2 = 0, 1; j_2 = 0) \rightarrow \text{Cl} + \text{H}_2\text{O}$  reaction as a function of translational energy and total energy. Adapted with permission from ref 183. Copyright 2014 American Institute of Physics.

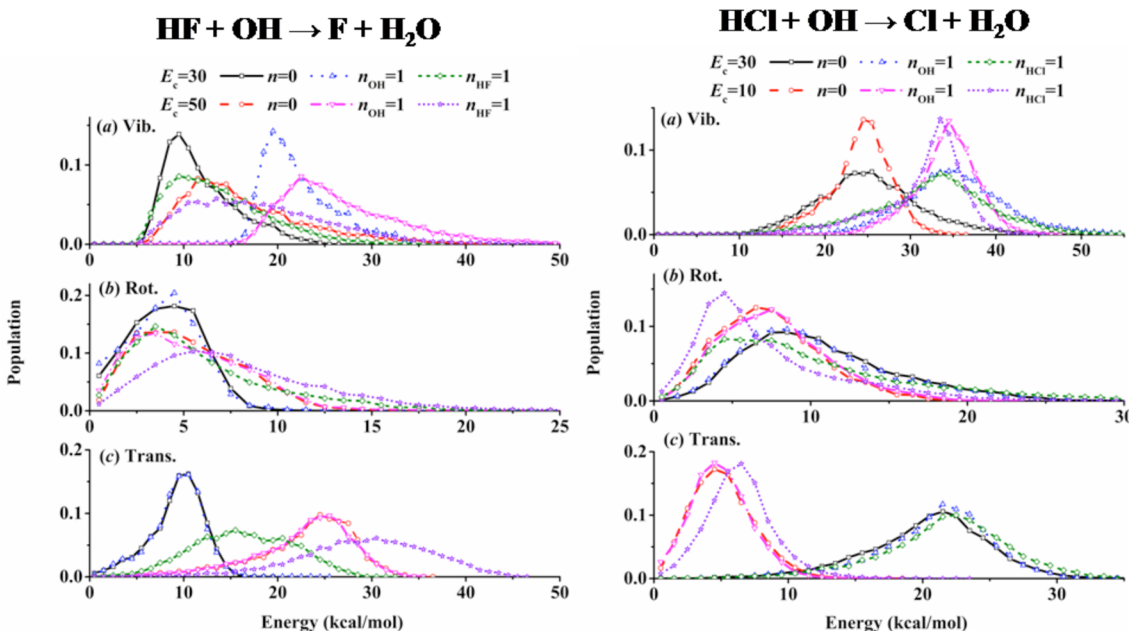


**Figure 7.** Normalized vibrational (*a*), rotational (*b*), and relative translational (*c*) energy distributions of  $\text{H}_2\text{O}$  for the reactions  $\text{HX} + \text{OH} \rightarrow \text{X} + \text{H}_2\text{O}$  with  $(n_{\text{HX}}, n_{\text{OH}}) = (0, 0), (0, 1), (1, 0)$  at  $E_c = 30$  and  $50$  kcal/mol for  $\text{X} = \text{F}$  (left side) and  $E_c = 30$  and  $10$  kcal/mol for  $\text{X} = \text{Cl}$  (right side). Adapted with permission from ref 184. Copyright 2015 American Institute of Physics.

consistent with the product energy disposal for the forward reaction.

More recently, the mode specific state-to-state reaction dynamics have been studied on the PIP-NN PES using both QCT<sup>184</sup> and QD methods.<sup>153</sup> In the QCT study, as shown in Figure 7, it was found that energy deposited in the HF vibration is effectively used to overcome the barrier of this endoergic reaction, while that imparted into the OH vibration is essentially transformed into the stretching modes of the  $\text{H}_2\text{O}$  product. This is again consistent with the SVP model, as the HF vibration is strongly coupled with the reaction coordinate while the OH vibration is almost orthogonal to the reaction coordinate. As a

result, increasing HF vibration leads to efficient energy flowing into the reaction coordinate, while the OH vibrational energy is sequestered and transferred adiabatically to the stretching vibrations of the  $\text{H}_2\text{O}$  product.

Very recently, the  $\text{F} + \text{HOD} \rightarrow \text{HF} + \text{OD}$  and  $\text{DF} + \text{OH}$  reactions have been investigated using an approximate QD method.<sup>185</sup> Because of the early barrier in this system, this reaction is unique for exploring bond-selective chemistry. Our results indicate that excitation of the local OH or OD vibrational mode enhances the cleavage of the corresponding bond. The bond selectivity is quite strong at low collision energies.

**V.B.  $\text{Cl} + \text{H}_2\text{O} \leftrightarrow \text{HCl} + \text{OH}$ .** Similar to the  $\text{F} + \text{H}_2\text{O}$  reaction, the  $\text{Cl} + \text{H}_2\text{O} \leftrightarrow \text{HCl} + \text{OH}$  reaction involves at least the three lowest-lying doublet electronic states. The degeneracies in the asymptotic regions are lifted by the spin-orbit couplings of Cl and OH radicals. Only the lowest  $^2\text{A}'$  state has been investigated. On the other hand, this reaction differs significantly from the  $\text{F} + \text{H}_2\text{O}$  reaction in several respects. In particular, the forward  $\text{Cl} + \text{H}_2\text{O}$  reaction is endoergic and, as a result, has a late or product-like barrier. As depicted in Figure 1, it is quite similar to the endoergic  $\text{H} + \text{H}_2\text{O}$  reaction.

The earlier PESs for this reactive system were either empirical, inaccurate, or limited in configuration space,<sup>186–191</sup> but they have facilitated several QCT<sup>192</sup> as well as reduced and full-dimensional QD calculations of the  $\text{Cl} + \text{H}_2\text{O} \leftrightarrow \text{HCl} + \text{OH}$  reaction.<sup>186–188,193–196</sup> The first ab initio based full-dimensional global PES for this reaction was reported by Li, Dawes, and Guo in 2013.<sup>197</sup> This LDG PES was also a PIP fit of  $\sim 25000$  MRCI/AVTZ points with a RMSE of  $279.8 \text{ cm}^{-1}$ . There is strong evidence showing that single-reference methods such as CCSD(T) are not appropriate for mapping out the global PES for this system because the transition-state region has unacceptable  $T_1$  values.<sup>197</sup> The forward barrier of  $20.53 \text{ kcal/mol}$  and reaction energy of  $17.44 \text{ kcal/mol}$  on the PIP-NN PES are also in good agreement with the best ab initio benchmarks,  $20.8$  and  $18.4 \text{ kcal/mol}$ , respectively.<sup>198</sup> The ab initio data was refitted recently using the PIP-NN approach, with the RMSE reduced to  $67.8 \text{ cm}^{-1}$ .<sup>199</sup> The PIP-NN PES is displayed in Figure 2 with respect to the Cl-H and O-H bond distances. The reaction profile for this reaction in Figure 1 also features pre- and post-reaction wells. These wells have similar bonding nature and geometry as those in the  $\text{F} + \text{H}_2\text{O}$  reaction.<sup>175</sup> However, the impact of the pre-reaction well is not expected to be significant here because of the high reaction barrier in the forward direction ( $20.53 \text{ kcal/mol}$ ). Neither is the spin-orbit correction, despite its larger amplitude. As a result, the PES was not spin-orbit corrected.

The rate coefficients for the forward  $\text{Cl} + \text{H}_2\text{O}$  reaction have been computed on the LDG PES with QCT,<sup>197</sup> and the results are in good agreement with both experimental and transition-state theory data. This endoergic reaction has a very small reaction cross section and low rate coefficients. QCT calculations with a collision energy of  $25 \text{ kcal/mol}$  indicated some rotational excitation in the HCl product, while the OH product is internally cold.<sup>197</sup> Furthermore, the calculated DCS is backward-dominated, although there exists a significant sideways scattering.<sup>197</sup>

The reverse  $\text{HCl} + \text{OH}$  reaction is exoergic and has recently been investigated using a QD method within the CS approximation.<sup>200</sup> While the OH vibrational excitation has little effect, interestingly, the HCl vibrational excitation enhances the reactivity more than translational excitation.<sup>200</sup> Since the reverse reaction has an early barrier, it presents another case that violates the extension of Polanyi's rules. As expected, however, the surprising vibrational mode specificity was consistent with the predictions of the SVP model.<sup>160</sup> Indeed, the strong promotional effect of the HCl vibration can be attributed to its strong coupling with the reaction coordinate at the transition state, evidenced by the large SVP value in Table 1. On the other hand, the SVP value for the OH vibration is almost zero, indicating its complete decoupling from the reaction coordinate. This picture is consistent with the spectator nature of the OH moiety in this reaction.

More recently, the bond selectivity of the  $\text{Cl} + \text{HOD}$  reaction has been studied using both QCT and QD (JS) methods on the PIP-NN PES.<sup>199</sup> The frequencies of the OH and OD stretching vibrations of HOD are well-separated within the local mode regime.<sup>164</sup> In agreement with experimental observations, the excitation of the O-H or O-D vibration in HOD greatly enhances the cleavage of the OH or OD bond, respectively. The calculated ICSs from both QD and QCT are in good agreement. In addition, the calculated OH/OD branching ratio was in quantitative agreement with experiment when the OH vibration was excited to  $n = 4$ .<sup>58</sup> Furthermore, the OD product is found to be internally cold while the HCl product possesses an inverted vibrational state distribution with a peak at  $n = 2$  at the experimental translational energy of  $3.97 \text{ kcal/mol}$ . Figure 8

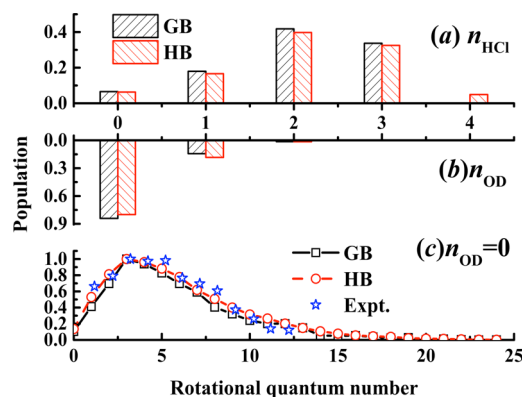


**Figure 8.** Normalized QCT vibrational state distributions of the (a) HCl and (b) OD products from the  $\text{Cl} + \text{HOD}(n_{\text{OH}} = 4) \rightarrow \text{HCl} + \text{OD}$  reaction and  $E_c = 1390 \text{ cm}^{-1}$ . The normalized rotational quantum state distributions of vibrationally ground state OD is also shown in (c). Adapted with permission from ref 199. Copyright 2015 Royal Society of Chemistry.

shows the QCT calculated product vibrational state distributions. The OD vibrational state distribution agrees with the experiment, but no experimental data are available for the HCl distribution. The binning method used in computing the vibrational state distributions has a small impact on the results. The OD product is found to be rotationally cold, which is consistent with the experiment, as shown in Figure 8, while the HCl product has moderate rotational excitation.

While a naive extension of Polanyi's rules predicts that reactant vibration would enhance the reactivity in this late-barrier reaction, they provide no guidance on bond selectivity. In contrast, the SVP model offers a clear picture of this issue. In Figure 9, the reactant normal modes and reaction coordinate vectors are shown along with their alignments. As shown in Table 1, the OH vibrational mode of HOD has a SVP value of 0.99, which essentially means that the vibrational coordinate is aligned near perfectly with the reaction coordinate at the Cl···HOD transition state for the  $\text{Cl} + \text{HOD} \rightarrow \text{HCl} + \text{OD}$  reaction. As a result, the energy imparted into the OH vibrational coordinate is equivalent to dumping energy directly in the reaction coordinate in the sudden limit, leading to a huge enhancement. Likewise, the energy in the OD vibration is effectively channeled into the reaction coordinate at the Cl···DOH transition state for the  $\text{Cl} + \text{HOD} \rightarrow \text{DCl} + \text{OH}$  reaction.

Our results revealed an additional finding for the reaction involving highly vibrationally excited HOD. It was shown that the reaction mechanism changes from direct abstraction to a

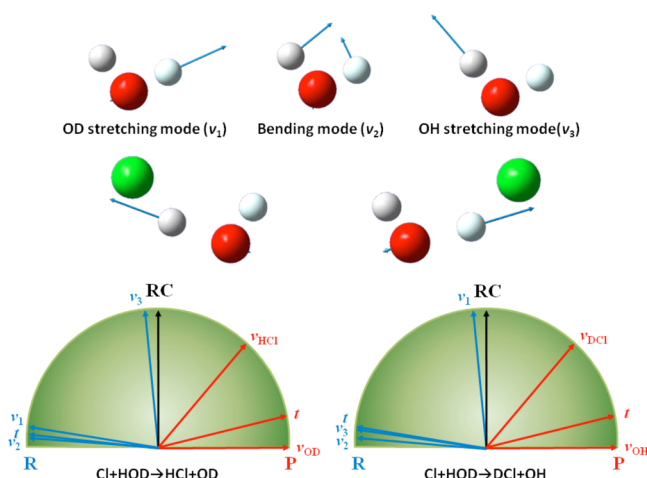


**Figure 9.** Normal mode vectors for the  $\text{Cl} + \text{HOD}$  reaction and the reaction coordinate vector at the transition state. The alignment of the reactant/product vectors with the reaction coordinate vector predicted by the SVP model is also shown.

capturelike one as the vibrational excitation increases.<sup>199</sup> This is evidenced in Figure 10 by the drastically increased reaction cross

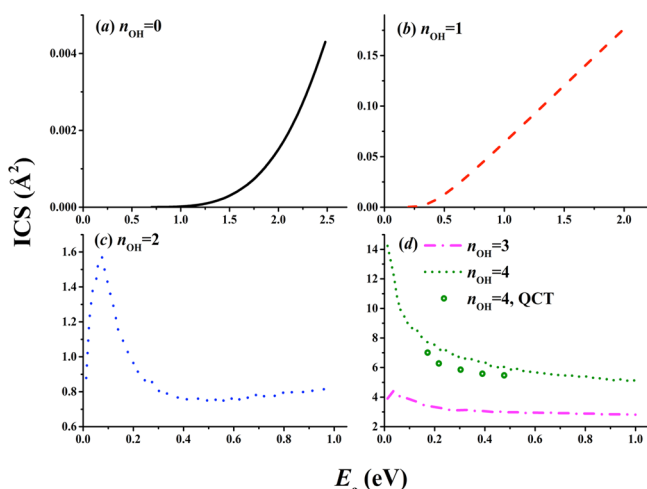


**Figure 10.** ICSs for the  $\text{Cl} + \text{HOD}$  ( $n_{\text{OH}} = 0, 1, 2, 3$ , and  $4$ )  $\rightarrow \text{HCl} + \text{OD}$  reaction obtained from  $J$ -shifting QD calculations. The QCT ICSs for  $n_{\text{OH}} = 4$  are also compared in (d). Note the vastly different scales of the panels. Adapted with permission from ref 199. Copyright 2015 Royal Society of Chemistry.

section and a change of the excitation function from a monotonically increasing function of energy to one that decays with energy. In addition, the differential cross section also changed from backward-biased to forward-biased. The latter energy dependence is characteristic of a barrierless complex-forming reaction.<sup>201</sup> Indeed, it was shown that the minimum energy path at the O–H turning point for highly vibrationally excited HOD is attractive, devoid of a barrier. This appears to be a general feature for activated reactions with vibrationally highly excited reactants.<sup>43</sup>

The state-to-state dynamics of the  $\text{HCl} + \text{OH} \rightarrow \text{Cl} + \text{H}_2\text{O}$  reaction has also been studied using a QCT method along with the  $\text{HF} + \text{OH} \rightarrow \text{F} + \text{H}_2\text{O}$  reaction.<sup>184</sup> Although both reactions produce the  $\text{H}_2\text{O}$  product, they have very different characteristics. Our QCT calculations showed that the  $\text{H}_2\text{O}$  product is

moderately excited in its three vibrational modes in the  $\text{HF} + \text{OH}$  reaction, but its stretching modes are highly excited in the  $\text{HCl} + \text{OH}$  reaction, consistent with the mode specificity of their corresponding reverse reactions. For both reactions, the OH reactant is essentially a spectator, which sequesters its energy throughout the reaction. On the other hand, the HF vibrational excitation has almost no impact on the  $\text{H}_2\text{O}$  vibrational distribution while HCl converts some of its vibrational energy into the stretching modes of  $\text{H}_2\text{O}$ . Figure 7 shows the corresponding distributions of the vibrational, rotational, and relative translational energy of the products  $\text{Cl} + \text{H}_2\text{O}$ . These mode specific correlations in these state-to-state dynamics can also be rationalized by the SVP model.

**V.C.  $\text{O}(\text{P}) + \text{H}_2\text{O} \leftrightarrow \text{OH} + \text{OH}$ .** In combustion, this endoergic reaction is a chain-branching step in its forward direction but a chain terminating event in the reverse direction. As a result, its kinetics have been extensively studied. The  $1^3A''$ ,  $1^3A'$ , and  $2^3A''$  states correlate adiabatically to both the reactants and products of this reaction and all have significant barriers.<sup>202</sup> Unlike the deeply bound singlet ground state of  $\text{HOOH}$ , the triplet states are all repulsive. Ab initio determination of the reaction barriers has been reported by several authors, and the rate coefficients have been determined using transition-state theory.<sup>203,204</sup> The lowest ( $1^3A''$ ) state PES has a late or product-like barrier, thus similar to the  $\text{H}/\text{Cl} + \text{H}_2\text{O}$  reactions, as depicted in Figure 1. Global PESs for the three lowest triplet states have been reported based on ab initio calculations,<sup>205,206</sup> and QCT calculations have been performed on these PESs to gain insights into the reaction dynamics.<sup>205,207,208</sup> However, there is evidence indicating that these PESs are not quantitatively accurate.<sup>204</sup> In 2013, Li and Guo (LG) reported a PIP PES for the lowest triplet state fitted to  $\sim 36000$  points calculated at the UCCSD(T)/AVTZ level of theory with an RMSE of  $383.5 \text{ cm}^{-1}$ .<sup>209</sup> (We note in passing that excited triplet state PESs are not amenable to the UCCSD(T) method, which is only applicable to the lowest triplet state.) The new LG PES, which has the same form as in the  $\text{F}/\text{Cl} + \text{H}_2\text{O}$  PESs discussed above,<sup>173,197</sup> has a barrier of  $20.32 \text{ kcal/mol}$ , close to the benchmark value of  $19.97 \text{ kcal/mol}$ .<sup>204</sup> The rate coefficients for the forward direction of this reaction were computed on this PES using both QCT and TST methods, and the agreement with both experiment and accurate theoretical data was excellent, thus validating the PES. In addition, the calculated rate coefficients for the reverse direction by the TST approach reproduce the experiment data except at temperatures lower than  $500 \text{ K}$ , which might be resulted from the neglect of the rather deep post-reaction well (compared to the rather low barrier in the reverse direction) in the reverse reaction.<sup>204</sup> The ab initio data were later refitted with the PIP-NN method.<sup>106</sup>

As shown in Figure 1, the reaction profile for this reaction on the lowest triplet state has a late barrier with a height of  $20.3 \text{ kcal/mol}$ , a pre-reaction well, and several post-reaction wells (see details in Figure 2 of ref 209). Interestingly, the forward reaction path from the reaction transition state leads to a nonlinear  $\text{HOOH}$  well, which is quite shallow. It can be readily converted to a hydrogen-bonded complex before the two products dissociate into the asymptote. QCT calculations for the forward reaction have been performed at  $25 \text{ kcal/mol}$  of collision energy. It was found that the DCS of this system is backward dominated, suggesting a direct rebound mechanism. This reaction presents an interesting case in which one of the OH products is a spectator while the other formed by the abstraction of the hydrogen from the water reactant is not. The QCT results clearly showed that the nonreactive OH product has a low rotational excitation, while

the newly formed OH product has a much higher rotational excitation. The latter also has a bimodal distribution, which was attributed to secondary collisions between the two OH products as they emerge from the transition state. At the collision energy studied, OH vibrational excitation was not allowed. However, the SVP model predicts that the newly formed OH product is inclined to have significant vibrational excitation, and the spectator OH should be internally cold.<sup>160</sup>

The mode specificity of the forward reaction on the lowest triplet state PES has been investigated using a QD method with the CS approximation,<sup>160</sup> and strong promotional effects by the stretching vibrational excitation of the H<sub>2</sub>O reactant were found. While both stretching modes are more effective than the translational mode, the symmetric stretching mode has a higher efficacy than the antisymmetric stretching mode. On the other hand, the bending excitation only enhances the reaction slightly. These observations are consistent with the SVP predictions in Table 1. Comparing with the F/Cl + H<sub>2</sub>O reactions, however, our understanding of the reaction dynamics of this reaction is much less complete than the two reactions discussed above. More work in this direction is planned.

**V.D. Other Related Systems.** Several authors have reported ab initio studies of other X + H<sub>2</sub>O  $\leftrightarrow$  XH + OH (X = Br, I) reactions and their reverse reactions.<sup>172,210–212</sup> These reactions are all endoergic in the forward direction and have very late barriers. In fact, the energy of the reactive saddle point is below the product asymptote. As can be expected, the dynamics of these reactions should be very similar to the Cl + H<sub>2</sub>O  $\leftrightarrow$  HCl + OH reaction. The current knowledge of the reaction dynamics is restricted to the OH + HBr  $\leftrightarrow$  Br + H<sub>2</sub>O reaction.<sup>187,193,213–216</sup> Using a PIP PES recently developed by Bowman and co-workers based on high-level ab initio data,<sup>210</sup> QCT studies of the OH + HBr reaction dynamics indicated strong excitations in all three vibrational modes of the H<sub>2</sub>O product,<sup>216</sup> similar to what we saw in the HCl + OH reaction.<sup>184</sup> In addition, the total cross section decays with the collision energy, in agreement with crossed molecular beam experiment.<sup>217</sup> This behavior is apparently due to the attractive PES in the entrance channel with a submerged barrier.<sup>210,216</sup>

## VI. CONCLUSIONS

The discussion above clearly illustrates the impressive progress that has been made in recent years for the prototypical X + H<sub>2</sub>O  $\leftrightarrow$  HX + OH reactions. This progress has been driven by developments in two areas. The first is based on advances in ab initio theory and fitting methods for constructing full-dimensional global PESs, and the second stems from the advances in quantum dynamical methods. The powerful combination of the two has enabled us to provide a quantitatively accurate characterization of the reaction dynamics. This level of accuracy is unprecedented and now allows us to address with confidence many important issues in these tetra-atomic reaction systems. They also form the basis for future advances in understanding other tetra-atomic reactions and reactions with even more atoms.

In this review, we have surveyed theoretical studies on the reactivity of both the forward and reverse directions of these reactions, with a focus on their mode specificity and bond selectivity. To understand these interesting phenomena uncovered by our dynamical studies on accurate PESs, we have taken advantage of a recently proposed SVP model, which attributes the dependence of reactivity on the excitation of a particular reactant mode to its coupling with the reaction coordinate at the transition state. The SVP model has been

demonstrated here and in other reactions to be generally reliable. Unlike Polanyi's rules for atom–diatom reactions, the SVP model is amenable to reactions with polyatomic reactants such as those discussed here. It has been shown to correctly predict mode specificity in several cases where a naive extension of Polanyi's rules failed. It is important to point out that the applicability of the SVP model is more general than gas phase bimolecular reactions. Recently, for example, it has been shown to predict mode specificity and bond selectivity in gas–surface reactions,<sup>218–221</sup> including those involving H<sub>2</sub>O,<sup>166,222,223</sup> which share many similarities with the gas-phase reactions discussed here. These developments suggest that our understanding of dynamics of gas phase and gas-surface reactions has advanced to a new level.

Finally, we note that the adiabatic model used in studying the reactions discussed here needs be improved by including nonadiabatic couplings. These nonadiabatic couplings include spin–orbit, derivative, and Renner–Teller interactions between a multitude of low-lying electronic states. Some experimental evidence has already been found to suggest the involvement of nonadiabatic dynamics in these reactions.<sup>55,56</sup> A rigorous QD treatment of the nonadiabatic dynamics remains a challenge.

The new theoretical methods discussed here are general and can be applied to larger systems.<sup>224–226</sup> As a result, we expect many more applications in the future. As internal excitations increase in energy, future studies will also have to address nonadiabatic dynamics among different electronic states. Apart from the mode specificity, it is of great interest to understand the steric effect in chemical reactions.<sup>10</sup> Better understanding of these issues will further advance our knowledge of chemical dynamics.

## ■ AUTHOR INFORMATION

### Corresponding Author

\*E-mail: hguo@unm.edu.

### Notes

The authors declare no competing financial interest.

### Biographies



Jun Li received his Ph.D. from Sichuan University, China, in 2011 with Prof. Xiangyuan Li. In 2009, he spent five months in National Chiao-Tung University with Prof. Sheng-Hsien Lin. After three years of postdoctoral research with Prof. Hua Guo at the University of New Mexico, he joined Chongqing University, China, as an Assistant Professor in September of 2014. His research interests include potential energy surfaces, reaction kinetics and dynamics, as well as photochemistry.



Bin Jiang received his Ph.D. at Nanjing University, China, in 2012 with Prof. Daiqian Xie. Since graduation, he has been a postdoctoral fellow with Prof. Hua Guo at University of New Mexico. He is interested in high-level ab initio potential energy surfaces and reaction dynamics in gas phase and/or at the gas–surface interface.



Bin Zhao received his Ph.D. degree from Nanyang Technological University, Singapore, in 2012 with Prof. Soo-Ying Lee. After visiting Prof. Uwe Manthe at the Universität Bielefeld, Germany, he currently conducts research as a Postdoctoral Research Fellow with Professor Hua Guo at The University of New Mexico. His research mainly focuses on chemical reaction dynamics in gas phase and the gas–surface interface and also on ultrafast nonlinear spectroscopy.



Hongwei Song is currently a Postdoctoral Research Fellow with Prof. Hua Guo at the University of New Mexico. He received his Ph.D. from Nanyang Technological University, Singapore, in 2012 with Prof. Soo-Ying Lee, and his research interests are in the areas of gas phase molecular reaction dynamics and spectroscopy.



Richard Dawes received his Ph.D. from the University of Manitoba (Canada) in 2005 before joining the group of Prof. Tucker Carrington Jr. as a postdoc at the Université de Montréal. In 2006, he worked with Prof. Donald L. Thompson (Missouri) on fitting PESs before joining Dr. Ahren W. Jasper at the Combustion Research Facility (Sandia, Livermore) in 2009. He became an Assistant Professor at the Missouri University of Science and Technology in 2010 and was granted an early career award by the U.S. Department of Energy in 2013. His research focuses on multistate multireference quantum chemistry and potential energy surfaces.



Jianyi Ma received his Ph.D. from Sichuan University, China, in 2009 with Prof. Xiangyuan Li. He was a postdoctoral fellow with Prof. Hua Guo at the University of New Mexico. In 2012, he joined the Institute of Atomic and Molecular Physics, Sichuan University, China, and is now a Professor of Physics. His research interests include reaction dynamics and combustion simulations.



Hua Guo did his undergraduate study at Chengdu Institute of Electronic Engineering, China. After receiving a M.S. degree with Prof. Guo-sen

Yan at Sichuan University, China, he moved in 1985 to the U.K. to pursue his D.Phil. degree at Sussex University under Prof. John N. Murrell, FRS. Following a postdoctoral appointment with Prof. George C. Schatz at Northwestern University, in 1988–1990, he started his independent career at the University of Toledo in 1990. He moved to the University of New Mexico in 1998 and is now Professor of Chemistry and Professor of Physics. He was elected Fellow of the American Physical Society in 2013. His research interests include reaction dynamics of reactions in the gas phase and at gas–surface interfaces, heterogeneous catalysis, and enzymatic reactions.

## ACKNOWLEDGMENTS

This material is based upon work supported by the U.S. Department of Energy, Office of Science, Office of Basic Energy Science under the Award DE-FG02-05ER15694 to H.G. and DE-SC0010616 to R.D. J.L. and J.M. also acknowledge partial support from the Hundred-Talent Foundation of Chongqing University (Grant 0220001104420 to J.L.) and the National Natural Science Foundation of China (Grant 91441107 to J.M.). We would like to thank our colleagues, in particular Joel Bowman, Bob Continetti, Jose Corchado, Joaquin Espinosa-Garcia, Bill Hase, Kopin Liu, Uwe Manthe, David Nesbitt, Fritz Schaefer, John Stanton, Al Wagner, Dick Zare, and Dong Hui Zhang for many useful discussions.

## REFERENCES

- (1) Casavecchia, P. Chemical Reaction Dynamics with Molecular Beams. *Rep. Prog. Phys.* **2000**, *63*, 355–414.
- (2) Liu, K. Crossed-Beam Studies of Neutral Reactions: State-Specific Differential Cross Sections. *Annu. Rev. Phys. Chem.* **2001**, *52*, 139–164.
- (3) Liu, K. Excitation Functions of Elementary Chemical Reactions: A Direct Link from Crossed-Beam Dynamics to Thermal Kinetics? *Int. Rev. Phys. Chem.* **2001**, *20*, 189–217.
- (4) Fernandez-Alonso, F.; Zare, R. N. Scattering Resonances in the Simplest Chemical Reactions. *Annu. Rev. Phys. Chem.* **2002**, *53*, 67–99.
- (5) Brouard, M.; O’Keeffe, P.; Vallance, C. Product State Resolved Dynamics of Elementary Reactions. *J. Phys. Chem. A* **2002**, *106*, 3629–3641.
- (6) Balucani, N.; Capozza, G.; Leonori, F.; Segoloni, E.; Casavecchia, P. Crossed Molecular Beam Reactive Scattering: From Simple Triatomic to Multichannel Polyatomic Reactions. *Int. Rev. Phys. Chem.* **2006**, *25*, 109–163.
- (7) Yang, X. State-to-State Dynamics of Elementary Bimolecular Reactions. *Annu. Rev. Phys. Chem.* **2007**, *58*, 433–459.
- (8) Crim, F. F. Chemical Dynamics of Vibrationally Excited Molecules: Controlling Reactions in Gases and on Surfaces. *Proc. Natl. Acad. Sci. U.S.A.* **2008**, *105*, 12654–12661.
- (9) Liu, K. Quantum Dynamical Resonances in Chemical Reactions: From A + BC to Polyatomic Systems. *Adv. Chem. Phys.* **2012**, *149*, 1–46.
- (10) Liu, K. Perspective: Vibrational-Induced Steric Effects in Bimolecular Reactions. *J. Chem. Phys.* **2015**, *142*, 080901.
- (11) Crim, F. F. Vibrational State Control of Bimolecular Reactions: Discovering and Directing the Chemistry. *Acc. Chem. Res.* **1999**, *32*, 877–884.
- (12) Crim, F. F. Molecular Reaction Dynamics across the Phases: Similarities and Differences. *Faraday Discuss.* **2012**, *157*, 9–26.
- (13) Crim, F. F. Bond-Selected Chemistry: Vibrational State Control of Photodissociation and Bimolecular Reaction. *J. Phys. Chem.* **1996**, *100*, 12725–12734.
- (14) Althorpe, S. C.; Clary, D. C. Quantum Scattering Calculations on Chemical Reactions. *Annu. Rev. Phys. Chem.* **2003**, *54*, 493–529.
- (15) Hu, W.; Schatz, G. C. Theories of Reactive Scattering. *J. Chem. Phys.* **2006**, *125*, 132301.
- (16) Polanyi, J. C. Concepts in Reaction Dynamics. *Acc. Chem. Res.* **1972**, *5*, 161–168.
- (17) Yoon, S.; Holiday, R. J.; Sibert, E. L., III; Crim, F. F. The Relative Reactivity of CH<sub>3</sub>D Molecules with Excited Symmetric and Antisymmetric Stretching Vibrations. *J. Chem. Phys.* **2003**, *119*, 9568–9575.
- (18) Liu, J.; Song, K.; Hase, W. L.; Anderson, S. L. Direct Dynamics Trajectory Study of Vibrational Effects: Can Polanyi Rules Be Generalized to a Polyatomic System? *J. Am. Chem. Soc.* **2004**, *126*, 8602–8603.
- (19) Yan, S.; Wu, Y.-T.; Liu, K. Tracking the Energy Flow Along the Reaction Path. *Proc. Natl. Acad. Sci. U.S.A.* **2008**, *105*, 12667–12672.
- (20) Zhang, J. Z. H.; Dai, J.; Zhu, W. Development of Accurate Quantum Dynamical Methods for Tetraatomic Reactions. *J. Phys. Chem.* **1997**, *101*, 2746–2754.
- (21) Zhang, D. H.; Collins, M. A.; Lee, S.-Y. First-Principles Theory for the H + H<sub>2</sub>O, D<sub>2</sub>O Reactions. *Science* **2000**, *290*, 961–963.
- (22) Zhang, D. H.; Yang, M.; Collins, M. A.; Lee, S.-Y. Probing the Transition State via Photoelectron and Photodetachment Spectroscopy of H<sub>3</sub>O<sup>−</sup>. *Proc. Natl. Acad. Sci. U.S.A.* **2002**, *99*, 11579–11582.
- (23) Xiao, C.; Xu, X.; Liu, S.; Wang, T.; Dong, W.; Yang, T.; Sun, Z.; Dai, D.; Xu, X.; Zhang, D. H.; et al. Experimental and Theoretical Differential Cross Sections for a Four-Atom Reaction: HD + OH → H<sub>2</sub>O + D. *Science* **2011**, *333*, 440–442.
- (24) Otto, R.; Ma, J.; Ray, A. W.; Daluz, J. S.; Li, J.; Guo, H.; Continetti, R. E. Imaging Dynamics on the F + H<sub>2</sub>O → HF + OH Potential Energy Surfaces from Wells to Barriers. *Science* **2014**, *343*, 396–399.
- (25) Manthe, U. Accurate Calculations of Reaction Rates: Predictive Theory Based on a Rigorous Quantum Transition State Concept. *Mol. Phys.* **2011**, *109*, 1415–1426.
- (26) Nyman, G.; Yu, H.-G. Quantum Approaches to Polyatomic Reaction Dynamics. *Int. Rev. Phys. Chem.* **2013**, *32*, 39–95.
- (27) Czakó, G.; Bowman, J. M. Reaction Dynamics of Methane with F, O, Cl, and Br on Ab Initio Potential Energy Surfaces. *J. Phys. Chem. A* **2014**, *118*, 2839–2864.
- (28) Schatz, G. C. A Quasiclassical Trajectory Study of Reagent Vibrational Excitation Effects in the OH+H<sub>2</sub>→H<sub>2</sub>O+H Reaction. *J. Chem. Phys.* **1981**, *74*, 1133–1139.
- (29) Sinha, A.; Hsiao, M. C.; Crim, F. F. Bond-Selected Bimolecular Chemistry: H + HOD(4v<sub>OH</sub>) → OD + H<sub>2</sub>. *J. Chem. Phys.* **1990**, *92*, 6333–6334.
- (30) Sinha, A.; Hsiao, M. C.; Crim, F. F. Controlling Bimolecular Reactions: Mode and Bond Selected Reaction of Water with Hydrogen Atoms. *J. Chem. Phys.* **1991**, *94*, 4928–4935.
- (31) Hsiao, M. C.; Sinha, A.; Crim, F. F. Energy Disposal in the Vibrational-State- and Bond-Selected Reaction of Water with Hydrogen Atoms. *J. Phys. Chem.* **1991**, *95*, 8263–8267.
- (32) Metz, R. B.; Thoemke, J. D.; Pfeiffer, J. M.; Crim, F. F. Selectively Breaking Either Bond in the Bimolecular Reaction of HOD with Hydrogen Atoms. *J. Chem. Phys.* **1993**, *99*, 1744–1751.
- (33) Bronikowski, M. J.; Simpson, W. R.; Girard, B.; Zare, R. N. Bond-Specific Chemistry: OD:OH Product Ratios for the Reactions H + HOD(100) and H + HOD(001). *J. Chem. Phys.* **1991**, *95*, 8647–8648.
- (34) Bronikowski, M. J.; Simpson, W. R.; Zare, R. N. Effect of Reagent Vibration on the H + HOD Reaction: An Example of Bond-Specific Chemistry. *J. Phys. Chem.* **1993**, *97*, 2194–2203.
- (35) Bronikowski, M. J.; Simpson, W. R.; Zare, R. N. Comparison of Reagent Stretch vs Bend Excitation in the H+ HOD Reaction: An Example of Mode Selective Chemistry. *J. Phys. Chem.* **1993**, *97*, 2204–2208.
- (36) Kudla, K.; Schatz, G. C. A Quasiclassical Trajectory Study of Bond Specific Chemistry in the Reaction H + HOD → H<sub>2</sub> + OH, HD + OH. *Chem. Phys. Lett.* **1992**, *193*, 507–511.
- (37) Kudla, K.; Schatz, G. C. A Quasiclassical Trajectory Study of Mode Specific Reaction Dynamics in the Cl + HOD and H + HOD Reactions. *Chem. Phys.* **1993**, *175*, 71–82.
- (38) Bowman, J. M.; Wang, D. Mode Selectivity in Reactions of H with HOD(100), HOD(001), and HOD(002). *J. Chem. Phys.* **1992**, *96*, 7852–7854.

- (39) Wang, D.; Bowman, J. M. Quantum Calculations of Mode Specificity in Reactions of H with HOD and H<sub>2</sub>O. *J. Chem. Phys.* **1993**, *98*, 6235–6247.
- (40) Clary, D. C. Bond-Selected Reaction of HOD with H Atoms. *Chem. Phys. Lett.* **1992**, *192*, 34–40.
- (41) Clary, D. C. Quantum Scattering Calculations on the OH + H<sub>2</sub>(v=0,1), OH+D<sub>2</sub>, and OD+H<sub>2</sub> Reactions. *J. Chem. Phys.* **1992**, *96*, 3656–3665.
- (42) Zhang, D. H.; Light, J. C. Mode Specificity in the H + HOD Reaction: Full-Dimensional Quantum Study. *J. Chem. Soc., Faraday Trans.* **1997**, *93*, 691–697.
- (43) Bene, E.; Lendvay, G.; Pota, G. Dynamics of Bimolecular Reactions of vibrationally Highly Excited Molecules: Quasiclassical Trajectory Studies. *J. Phys. Chem. A* **2005**, *109*, 8336–8340.
- (44) Jiang, B.; Xie, D.; Guo, H. Calculation of Multiple Initial State Selected Reaction Probabilities from Chebyshev Correlation Functions. Influence of Reactant Rotational and Vibrational Excitation on Reaction H + H<sub>2</sub>O → OH + H<sub>2</sub>. *J. Chem. Phys.* **2011**, *135*, 084112.
- (45) Fu, B.; Zhang, D. H. Mode Specificity in the H + H<sub>2</sub>O → H<sub>2</sub> + OH Reaction: A Full-Dimensional Quantum Dynamics Study. *J. Chem. Phys.* **2013**, *138*, 184308.
- (46) Fu, B.; Zhang, D. H. A Full-Dimensional Quantum Dynamics Study of the Mode Specificity in the H + HOD Abstraction Reaction. *J. Chem. Phys.* **2015**, *142*, 064314.
- (47) Schatz, G. C.; Elgersma, H. A Quasi-Classical Trajectory Study of Product Vibrational Distributions in the OH + H<sub>2</sub> → H<sub>2</sub>O + H Reaction. *Chem. Phys. Lett.* **1980**, *73*, 21–25.
- (48) Wu, G.-S.; Schatz, G. C.; Lendvay, G.; Fang, D. C.; Harding, L. B. A New Potential Surface and Quasiclassical Trajectory Study of H + H<sub>2</sub>O → OH + H<sub>2</sub>. *J. Chem. Phys.* **2000**, *113*, 3150–3161.
- (49) Yang, M.; Zhang, D. H.; Collins, M. A.; Lee, S.-Y. Ab Initio Potential-Energy Surface for the Reactions OH + H<sub>2</sub> → H<sub>2</sub>O + H. *J. Chem. Phys.* **2001**, *115*, 174–178.
- (50) Yang, M.; Zhang, D. H.; Collins, M. A.; Lee, S.-Y. Quantum Dynamics on New Potential Energy Surfaces for the H<sub>2</sub> + OH → H<sub>2</sub>O + H Reaction. *J. Chem. Phys.* **2001**, *114*, 4759–4762.
- (51) Chen, J.; Xu, X.; Zhang, D. H. A Global Potential Energy Surface for the H<sub>2</sub> + OH ↔ H<sub>2</sub>O + H Reaction Using Neural Networks. *J. Chem. Phys.* **2013**, *138*, 154301.
- (52) Duewer, W. H.; Setser, D. W. Infrared Chemiluminescence and Energy Partitioning from Reactions of Fluorine Atoms with Hydrides of Carbon, Silicon, Oxygen, Sulfur, Nitrogen, and Phosphorus. *J. Chem. Phys.* **1973**, *58*, 2310–2320.
- (53) Agrawalla, B. S.; Setser, D. W. Infrared Chemiluminescence and Laser-Induced Fluorescence Studies of Energy Disposal by Reactions of F-Atoms and Cl-Atoms with H<sub>2</sub>S (D<sub>2</sub>S), H<sub>2</sub>Se, H<sub>2</sub>O (D<sub>2</sub>O), and CH<sub>3</sub>OH. *J. Phys. Chem.* **1986**, *90*, 2450–2462.
- (54) Zolot, A. M.; Nesbitt, D. J. Crossed Jet Reactive Scattering Dynamics of F + H<sub>2</sub>O → HF(v,j) + OH(v,j): HF(v,j) Product Quantum State Distributions under Single-Collision Conditions. *J. Chem. Phys.* **2008**, *129*, 184305.
- (55) Ziemkiewicz, M.; Wojcik, M.; Nesbitt, D. J. Direct Evidence for Non-Adiabatic Dynamics in Atom+Polyatom Reactions: Crossed-Jet Laser Studies of F + D<sub>2</sub>O → DF + OD. *J. Chem. Phys.* **2005**, *123*, 224307.
- (56) Ziemkiewicz, M.; Nesbitt, D. J. Nonadiabatic Reactive Scattering in Atom+Triatom Systems: Nascent Rovibronic Distributions in F + H<sub>2</sub>O → HF + OH. *J. Chem. Phys.* **2009**, *131*, 054309.
- (57) Sinha, A.; Thoemke, J. D.; Crim, F. F. Controlling Bimolecular Reactions: Mode and Bond Selected Reaction of Water with Translationally Energetic Chlorine Atoms. *J. Chem. Phys.* **1992**, *96*, 372–376.
- (58) Thoemke, J. D.; Pfeiffer, J. M.; Metz, R. B.; Crim, F. F. Mode-Selective and Bond-Selective Reactions of Chlorine Atoms with Highly vibrationally Excited H<sub>2</sub>O and HOD. *J. Phys. Chem.* **1995**, *99*, 13748–13754.
- (59) Pfeiffer, J. M.; Woods, E.; Metz, R. B.; Crim, F. F. Probing the New Bond in the vibrationally Controlled Bimolecular Reaction of O with HOD(4v<sub>OH</sub>). *J. Chem. Phys.* **2000**, *113*, 7982–7987.
- (60) Butkovskaya, N. I.; Setser, D. W. Vibrational Excitation of H<sub>2</sub>O and HOD Molecules Produced by Reactions of OH and OD with cyclo-C<sub>6</sub>H<sub>12</sub>, n-C<sub>4</sub>H<sub>10</sub>, neo-C<sub>5</sub>H<sub>12</sub>, HCl, DCl, and NH<sub>3</sub> as Studied by Infrared Chemiluminescence. *J. Chem. Phys.* **1998**, *108*, 2434–2477.
- (61) Orient, O. J.; Chutjian, A.; Murad, E. Reaction and Electronic Excitation in Crossed-Beams Collisions of Low-Energy O(<sup>3</sup>P) Atoms with H<sub>2</sub>O and CO<sub>2</sub>. *Phys. Rev. Lett.* **1990**, *65*, 2359–2361.
- (62) Brunsvoold, A. L.; Zhang, J.; Upadhyaya, H. P.; Minton, T. K.; Camden, J. P.; Paci, J. T.; Schatz, G. C. Crossed-Beams and Theoretical Studies of the O(<sup>3</sup>P) + H<sub>2</sub>O → HO<sub>2</sub> + H Reaction Excitation Function. *J. Phys. Chem. A* **2007**, *111*, 10907–10913.
- (63) Arnold, D. W.; Xu, C.; Neumark, D. M. Spectroscopy of the Transition State: Elementary Reactions of the Hydroxyl Radical Studied by Photoelectron Spectroscopy of O<sup>−</sup>(H<sub>2</sub>O) and H<sub>3</sub>O<sup>−</sup>. *J. Chem. Phys.* **1995**, *102*, 6088–6099.
- (64) Deyerl, H.-J.; Clements, T. G.; Luong, A. K.; Continetti, R. E. Transition State Dynamics of the OH + OH → O + H<sub>2</sub>O Reaction Studies by Dissociative Photodetachment of H<sub>2</sub>O<sup>−</sup>. *J. Chem. Phys.* **2001**, *115*, 6931–6940.
- (65) Yang, X.; Wang, X. B.; Wang, L. S. Photodetachment of F<sup>−</sup>(H<sub>2</sub>O)<sub>N</sub> (N=1–4): Observation of Charge-Transfer States [F<sup>−</sup>(H<sub>2</sub>O)<sub>N</sub><sup>+</sup>] and the Transition State of F+H<sub>2</sub>O Hydrogen Abstraction Reaction. *J. Chem. Phys.* **2001**, *115*, 2889–2892.
- (66) Truhlar, D. G.; Muckerman, J. T. Reactive Scattering Cross Sections III: Quasiclassical and Semiclassical Methods. In *Atom-Molecule Collision Theory*, Bernstein, R. B., Ed.; Plenum: New York, 1979; pp 505–566.
- (67) Schatz, G. C. Quasiclassical Trajectory Studies of State-Resolved Bimolecular Reactions: Vibrational Distributions in Triatomic Products. *J. Phys. Chem.* **1995**, *99*, 516–524.
- (68) Hase, W. L. Classical Trajectory Simulations: Initial Conditions. In *Encyclopedia of Computational Chemistry*, Alinger, N. L., Ed.; Wiley: New York, 1998; Vol. 1, pp 399–402.
- (69) Hase, W. L.; Song, K.; Gordon, M. S. Direct Dynamics Simulations. *Comput. Sci. Eng.* **2003**, *5*, 36–44.
- (70) Dawes, R.; Lolur, P.; Li, A.; Jiang, B.; Guo, H. Communication: An Accurate Global Potential Energy Surface for the Ground Electronic State of Ozone. *J. Chem. Phys.* **2013**, *139*, 201103.
- (71) Sathyamurthy, N.; Raff, L. M. Quasiclassical Trajectory Studies Using 3D Spline Interpolation of Ab Initio Surfaces. *J. Chem. Phys.* **1975**, *63*, 464–473.
- (72) Xu, C.; Xie, D.; Zhang, D. H.; Lin, S. Y.; Guo, H. A New Ab Initio Potential Energy Surface of HO<sub>2</sub>(X<sup>2</sup>A') and Quantum Studies of HO<sub>2</sub> Vibrational Spectrum and Rate Constants for the H + O<sub>2</sub> ↔ O + OH Reactions. *J. Chem. Phys.* **2005**, *122*, 244305.
- (73) Hollebeek, T.; Ho, T.-S.; Rabitz, H. Constructing Multidimensional Molecular Potential Energy Surfaces from Ab Initio Data. *Annu. Rev. Phys. Chem.* **1999**, *50*, 537–570.
- (74) Dawes, R.; Thompson, D. L.; Wagner, A. F.; Minkoff, M. Interpolating Moving Least-Squares Methods for Fitting Potential Energy Surfaces: A Strategy for Efficient Automatic Data Point Placement in High Dimensions. *J. Chem. Phys.* **2008**, *128*, 084107.
- (75) Dawes, R.; Thompson, D. L.; Wagner, A. F.; Minkoff, M. Ab Initio Wavenumber Accurate Spectroscopy: CH<sub>2</sub> and HCN Vibrational Levels on Automatically Generated Imls Potential Energy Surface. *J. Phys. Chem. A* **2009**, *113*, 4709–4721.
- (76) Dawes, R.; Wang, X.-G.; Jasper, A. W.; Carrington, T., Jr. Nitrous Oxide Dimer: A New Potential Energy Surface and Rovibrational Spectrum of the Nonpolar Isomer. *J. Chem. Phys.* **2010**, *133*, 134304.
- (77) Ischtwan, J.; Collins, M. A. Molecular Potential Energy Surfaces by Interpolation. *J. Chem. Phys.* **1994**, *100*, 8080–8088.
- (78) Collins, M. A. Molecular Potential-Energy Surfaces for Chemical Reaction Dynamics. *Theor. Chem. Acc.* **2002**, *108*, 313–324.
- (79) Murrell, J. N.; Carter, S.; Farantos, S. C.; Huxley, P.; Varandas, A. J. C. *Molecular Potential Energy Functions*; Wiley: Chichester, 1984.
- (80) Varandas, A. J. C. Intermolecular and Intramolecular Potentials. *Adv. Chem. Phys.* **1988**, *74*, 255–338.
- (81) Jackle, A.; Meyer, H.-D. Product Representation of Potential Energy Surfaces. *J. Chem. Phys.* **1996**, *104*, 7974–7984.

- (82) Carter, S.; Culik, S. J.; Bowman, J. M. Vibrational Self-Consistent Field Method for Many-Mode Systems: A New Approach and Application to the Vibrations of CO Adsorbed on Cu(100). *J. Chem. Phys.* **1997**, *107*, 10458–10469.
- (83) Li, G.; Rosenthal, C.; Rabitz, H. High Dimensional Model Representations. *J. Phys. Chem. A* **2001**, *105*, 7765–7777.
- (84) Xie, Z.; Bowman, J. M. Permutationally Invariant Polynomial Basis for Molecular Energy Surface Fitting Via Monomial Symmetrization. *J. Chem. Theory Comput.* **2010**, *6*, 26–34.
- (85) Braams, B. J.; Bowman, J. M. Permutationally Invariant Potential Energy Surfaces in High Dimensionality. *Int. Rev. Phys. Chem.* **2009**, *28*, 577–606.
- (86) Bowman, J. M.; Czakó, G.; Fu, B. High-Dimensional Ab Initio Potential Energy Surfaces for Reaction Dynamics Calculations. *Phys. Chem. Chem. Phys.* **2011**, *13*, 8094–8111.
- (87) Raff, L. M.; Komanduri, R.; Hagan, M.; Bukkapatnam, S. T. S. *Neural Networks in Chemical Reaction Dynamics*; Oxford University Press: Oxford, 2012.
- (88) Behler, J. Neural Network Potential-Energy Surfaces in Chemistry: A Tool for Large-Scale Simulations. *Phys. Chem. Chem. Phys.* **2011**, *13*, 17930–17955.
- (89) Hagan, M. T.; Menhaj, M. B. Training Feedforward Networks with the Marquardt Algorithm. *IEEE Transactions on Neural Networks* **1994**, *5*, 989–993.
- (90) Beale, M. H.; Hagan, M. T.; Demuth, H. B. *Neural Network Toolbox 7 User's Guide*; The MathWorks, Inc.: Natick, MA, 2010.
- (91) Zhou, Z.-H.; Wu, J.; Tang, W. Ensembling Neural Networks: Many Could Be Better Than All. *Artificial Intelligence* **2002**, *137*, 239–263.
- (92) Handley, C. M.; Popelier, P. L. A. Potential Energy Surfaces Fitted by Artificial Neural Networks. *J. Phys. Chem. A* **2010**, *114*, 3371–3383.
- (93) Manzhos, S.; Dawes, R.; Carrington, T. Neural Network-Based Approaches for Building High Dimensional and Quantum Dynamics-Friendly Potential Energy Surfaces, *Int. J. Quantum Chem.* **2014**, in press, 10.1002/qua.24795.
- (94) Bunker, P. R.; Jensen, P. *Molecular Symmetry and Spectroscopy*. NRC Research Press: Ottawa, 1998.
- (95) Chen, J.; Xu, X.; Xu, X.; Zhang, D. H. Communication: An Accurate Global Potential Energy Surface for the OH + CO → H + CO<sub>2</sub> Reaction Using Neural Networks. *J. Chem. Phys.* **2013**, *138*, 221104.
- (96) Majumder, M.; Hegger, S. E.; Dawes, R.; Manzhos, S.; Wang, X.-G.; Carrington Jr., T.; Li, J.; Guo, H. Explicitly-Correlated MRCI-F12 Potential Energy Surfaces for Methane Fit with Several Permutation Invariant Schemes and Full-Dimensional Vibrational Calculations. *Mol. Phys.* **2015**, in press, 10.1080/00268976.2015.1015642.
- (97) Ludwig, J.; Vlachos, D. G. Ab Initio Molecular Dynamics of Hydrogen Dissociation on Metal Surfaces Using Neural Networks and Novelty Sampling. *J. Chem. Phys.* **2007**, *127*, 154716.
- (98) Le, M. H.; Huynh, S.; Raff, L. M. Molecular Dissociation of Hydrogen Peroxide (HOOH) on a Neural Network Ab Initio Potential Surface with a New Configuration Sampling Method Involving Gradient Fitting. *J. Chem. Phys.* **2009**, *131*, 014107.
- (99) Le, H. M.; Raff, L. M. Molecular Dynamics Investigation of the Bimolecular Reaction BeH + H<sub>2</sub> → BeH<sub>2</sub> + H on an Ab Initio Potential-Energy Surface Obtained Using Neural Network Methods with Both Potential and Gradient Accuracy Determination. *J. Phys. Chem. A* **2010**, *114*, 45–53.
- (100) Prudente, F. V.; Acioli, P. H.; Soares Neto, J. J. The Fitting of Potential Energy Surfaces Using Neural Networks: Application to the Study of Vibrational Levels of H<sub>3</sub><sup>+</sup>. *J. Chem. Phys.* **1998**, *109*, 8801–8808.
- (101) Nguyen, H. T. T.; Le, H. M. Modified Feed-Forward Neural Network Structures and Combined-Function-Derivative Approximations Incorporating Exchange Symmetry for Potential Energy Surface Fitting. *J. Phys. Chem. A* **2012**, *116*, 4629–4638.
- (102) Gassner, H.; Probst, M.; Lauenstein, A.; Hermansson, K. Representation of Intermolecular Potential Functions by Neural Networks. *J. Phys. Chem. A* **1998**, *102*, 4596–4605.
- (103) Lorenz, S.; Scheffler, M.; Gross, A. Descriptions of Surface Chemical Reactions Using a Neural Network Representation of the Potential-Energy Surface. *Phys. Rev. B* **2006**, *73*, 115431.
- (104) Behler, J.; Lorenz, S.; Reuter, K. Representing Molecule-Surface Interactions with Symmetry-Adapted Neural Networks. *J. Chem. Phys.* **2007**, *127*, 014705.
- (105) Jiang, B.; Guo, H. Permutation Invariant Polynomial Neural Network Approach to Fitting Potential Energy Surfaces. *J. Chem. Phys.* **2013**, *139*, 054112.
- (106) Li, J.; Jiang, B.; Guo, H. Permutation Invariant Polynomial Neural Network Approach to Fitting Potential Energy Surfaces. II. Four-Atomic Systems. *J. Chem. Phys.* **2013**, *139*, 204103.
- (107) Schmelzer, A.; Murrell, J. N. The General Analytic-Expression for S<sub>4</sub> Symmetry Invariant Potential Energy Functions of Tetra-Atomic Homonuclear Molecules. *Int. J. Quantum Chem.* **1985**, *28*, 287–295.
- (108) Ischwan, J.; Collins, M. A. Symmetry-Invariant Reaction-Path Potentials. *J. Chem. Phys.* **1991**, *94*, 7084–7097.
- (109) Derksen, H.; Kemper, G. *Computational Invariant Theory*; Springer-Verlag: Berlin, 2002.
- (110) Hamermesh, M. *Group Theory*; Addison-Wesley: Reading, MA, 1962.
- (111) Bartlett, R. J.; Musial, M. Coupled-Cluster Theory in Quantum Chemistry. *Rev. Mod. Phys.* **2007**, *79*, 291–352.
- (112) Lee, T. J. Comparison of the T<sub>1</sub> and D<sub>1</sub> Diagnostics for Electronic Structure Theory: A New Definition for the Open-Shell D<sub>1</sub> Diagnostic. *Chem. Phys. Lett.* **2003**, *372*, 362–367.
- (113) Werner, H.-J. Matrix-Formulated Direct Multiconfiguration Self-Consistent Field and Multiconfiguration Reference Configuration-Interaction Methods. *Adv. Chem. Phys.* **1987**, *69*, 1–62.
- (114) Kong, L.; Bischoff, F. A.; Valeev, E. F. Explicitly Correlated R12/F12 Methods for Electronic Structure. *Chem. Rev.* **2011**, *112*, 75–107.
- (115) Kendall, R. A.; Dunning, T. H.; Harrison, R. J. Electron Affinities of the First-Row Atoms Revisited. Systematic Basis Sets and Wave Functions. *J. Chem. Phys.* **1992**, *96*, 6796–6806.
- (116) Alexander, M. H.; Manolopoulos, D. E.; Werner, H.-J. An Investigation of the F+H<sub>2</sub> Reaction Based on a Full Ab Initio Description of the Open-Shell Character of the F(<sup>2</sup>P) Atom. *J. Chem. Phys.* **2000**, *113*, 11084–11100.
- (117) Czakó, G.; Bowman, J. M. An Ab Initio Spin-Orbit-Corrected Potential Energy Surface and Dynamics for the F+CH<sub>4</sub> and F + CHD<sub>3</sub> Reactions. *Phys. Chem. Chem. Phys.* **2011**, *13*, 8306–8312.
- (118) Li, J.; Wang, Y.; Jiang, B.; Ma, J.; Dawes, R.; Xie, D.; Bowman, J. M.; Guo, H. Communication: A Chemically Accurate Global Potential Energy Surface for the HO + CO → H + CO<sub>2</sub> Reaction. *J. Chem. Phys.* **2012**, *136*, 041103.
- (119) Xie, C.; Li, J.; Xie, D.; Guo, H. Quasi-Classical Trajectory Study of the H + CO<sub>2</sub> → HO + CO Reaction on a New Ab Initio Based Potential Energy Surface. *J. Chem. Phys.* **2012**, *137*, 024308.
- (120) Jiang, B.; Guo, H. Permutation Invariant Polynomial Neural Network Approach to Fitting Potential Energy Surfaces. III. Molecule-Surface Interactions. *J. Chem. Phys.* **2014**, *141*, 034109.
- (121) Corchado, J. C.; Espinosa-Garcia, J. Product Vibrational Distributions in Polyatomic Species Based on Quasiclassical Trajectory Calculations. *Phys. Chem. Chem. Phys.* **2009**, *11*, 10157–10164.
- (122) Bonnet, L. Classical Dynamics of Chemical Reactions in a Quantum Spirit. *Int. Rev. Phys. Chem.* **2013**, *32*, 171–228.
- (123) Zhang, J. Z. H. *Theory and Application of Quantum Molecular Dynamics*; World Scientific: Singapore, 1999.
- (124) Zhang, D. H.; Zhang, J. Z. H. Full-Dimensional Time-Dependent Treatment for Diatom-Diatom Reactions: The H<sub>2</sub>+OH Reaction. *J. Chem. Phys.* **1994**, *101*, 1146–1156.
- (125) Zare, R. N. *Angular Momentum*; Wiley: New York, 1988.
- (126) Chen, R.; Ma, G.; Guo, H. Full-Dimensional Calculation of Vibrational Spectrum of Hydrogen Peroxide (HOOH). *Chem. Phys. Lett.* **2000**, *320*, 567–574.
- (127) Jiang, B.; Guo, H. Competition between Abstraction and Exchange Channels in H + HCN Reaction: Full-Dimensional Quantum Dynamics. *J. Chem. Phys.* **2013**, *139*, 224310.

- (128) Sun, Z.; Yang, W.; Zhang, D. H. Higher-Order Split Operator Schemes for Solving the Schrodinger Equation in the Time-Dependent Wave Packet Method: Applications to Triatomic Reactive Scattering Calculations. *Phys. Chem. Chem. Phys.* **2012**, *14*, 1827–1845.
- (129) Guo, H., Chebyshev Propagation and Applications to Scattering Problems. In *Theory of Chemical Reaction Dynamics*, Lagana, A., Lendvay, G., Eds.; Kluwer: Dordrecht, 2004; pp 217–229.
- (130) Lin, S. Y.; Guo, H. Full-Dimensional Wave Packet Studies of Vibrational Relaxation of Both Para and Ortho-H<sub>2</sub>. *J. Phys. Chem. A* **2003**, *107*, 7197–7203.
- (131) Ma, J.; Li, J.; Guo, H. Quantum Dynamics of the HO + CO → H + CO<sub>2</sub> Reaction on an Accurate Potential Energy Surface. *J. Phys. Chem. Lett.* **2012**, *3*, 2482–2486.
- (132) Althorpe, S. C. Quantum Wavepacket Method for State-to-State Reactive Cross-Sections. *J. Chem. Phys.* **2001**, *114*, 1601–1616.
- (133) Lin, S. Y.; Guo, H. Quantum State-to-State Cross Sections for Atom-Diatom Reactions, a Chebyshev Real Wave Packet Approach. *Phys. Rev. A* **2006**, *74*, 022703.
- (134) Sun, Z.; Guo, H.; Zhang, D. H. Extraction of State-to-State Reactive Scattering Attributes from Wave Packet in Reactant Jacobi Coordinates. *J. Chem. Phys.* **2010**, *132*, 084112.
- (135) Mandelshtam, V. A.; Taylor, H. S. A Simple Recursion Polynomial Expansion of the Green's Function with Absorbing Boundary Conditions. Application to the Reactive Scattering. *J. Chem. Phys.* **1995**, *103*, 2903–2907.
- (136) Chen, R.; Guo, H. Evolution of Quantum System in Order Domain of Chebychev Operator. *J. Chem. Phys.* **1996**, *105*, 3569–3578.
- (137) Gray, S. K.; Balint-Kurti, G. G. Quantum Dynamics with Real Wavepackets, Including Application to Three-Dimensional ( $J=0$ ) D + H<sub>2</sub> → HD + H Reactive Scattering. *J. Chem. Phys.* **1998**, *108*, 950–962.
- (138) Sun, Z.; Lee, S.-Y.; Guo, H.; Zhang, D. H. Comparison of Second-Order Split Operator and Chebyshev Propagator in Wave Packet Based State-to-State Reactive Scattering Calculations. *J. Chem. Phys.* **2009**, *130*, 174102.
- (139) Light, J. C.; Carrington, T., Jr. Discrete-Variable Representations and Their Utilization. *Adv. Chem. Phys.* **2000**, *114*, 263–310.
- (140) Pack, R. T. Space-Fixed Vs Body-Fixed Axes in Atom-Diatom Molecule Scattering. Sudden Approximations. *J. Chem. Phys.* **1974**, *60*, 633–639.
- (141) McGuire, P.; Kouri, D. J. Quantum Mechanical Close Coupling Approach to Molecular Collisions.  $J_z$ -Conserving Coupled States Approximation. *J. Chem. Phys.* **1974**, *60*, 2488–2499.
- (142) Lin, S. Y.; Guo, H. Quantum Wave Packet Study of Reactive and Inelastic Scattering between C(<sup>1</sup>D) and H<sub>2</sub>. *J. Chem. Phys.* **2003**, *119*, 11602–11608.
- (143) Bowman, J. M. Reduced Dimensionality Theory of Quantum Reactive Scattering. *J. Phys. Chem.* **1991**, *95*, 4960–4968.
- (144) Zhang, D. H.; Xie, D.; Yang, M. State-to-State Integral Cross-Section for the H + H<sub>2</sub>O → H<sub>2</sub> + OH Abstraction Reaction. *Phys. Rev. Lett.* **2002**, *89*, 283203.
- (145) Zhang, D. H. State-to-State Quantum Reactive Scattering for Four-Atom Chemical Reactions: Differential Cross Section for the H + H<sub>2</sub>O → H<sub>2</sub> + OH Abstraction Reaction. *J. Chem. Phys.* **2006**, *125*, 133102.
- (146) Peng, T.; Zhang, J. Z. H. A Reactant-Product Decoupling Method for State-to-State Reactive Scattering. *J. Chem. Phys.* **1996**, *105*, 6072–6074.
- (147) Althorpe, S. C.; Kouri, D. J.; Hoffman, D. K.; Zhang, J. Z. H. Reactant-Product Decoupling Approach to State-Resolved Reactive Scattering: Time-Independent Wavepacket Formulation. *J. Chem. Soc., Faraday Trans.* **1997**, *93*, 703–708.
- (148) Cvitaš, M. T.; Althorpe, S. C. A Chebyshev Method for State-to-State Reactive Scattering Using Reactant-Product Decoupling: OH + H<sub>2</sub> → H<sub>2</sub>O + H. *J. Chem. Phys.* **2013**, *139*, 064307.
- (149) Welsch, R.; Huarte-Larrañaga, F.; Manthe, U. State-to-State Reaction Probabilities within the Quantum Transition State Framework. *J. Chem. Phys.* **2012**, *136*, 064117.
- (150) Welsch, R.; Manthe, U. Thermal Flux Based Analysis of State-to-State Reaction Probabilities. *Mol. Phys.* **2012**, *110*, 703–715.
- (151) Welsch, R.; Manthe, U. Loss of Memory in H + CH<sub>4</sub> → H<sub>2</sub> + CH<sub>3</sub> State-to-State Reactive Scattering. *J. Phys. Chem. Lett.* **2015**, *6*, 338–342.
- (152) Zhao, B.; Sun, Z.; Guo, H. Calculation of the State-to-State S-Matrix for Tetra-Atomic Reactions with Transition-State Wave Packets: H<sub>2</sub>/D<sub>2</sub> + OH → H/D + H<sub>2</sub>O/HOD. *J. Chem. Phys.* **2014**, *141*, 154112.
- (153) Zhao, B.; Guo, H. Modulations of Transition-State Control of State-to-State Dynamics of the F + H<sub>2</sub>O → HF + OH Reaction. *J. Phys. Chem. Lett.* **2015**, *6*, 676–680.
- (154) Zhao, B.; Sun, Z.; Guo, H. Calculation of State-to-State Differential and Integral Cross Sections for Atom-Diatom Reactions with Transition-State Wave Packets. *J. Chem. Phys.* **2014**, *140*, 234110.
- (155) Miller, W. H. Quantum Mechanical Transition State Theory and a New Semiclassical Model for Reaction Rate Constants. *J. Chem. Phys.* **1974**, *61*, 1823–1834.
- (156) Miller, W. H.; Schwartz, S. D.; Tromp, J. W. Quantum Mechanical Rate Constants for Bimolecular Reactions. *J. Chem. Phys.* **1983**, *79*, 4889–4899.
- (157) Park, T. P.; Light, J. C. Quantum Flux Operators and Thermal Rate Constant: Collinear H+H<sub>2</sub>. *J. Chem. Phys.* **1988**, *88*, 4897–4912.
- (158) Matzkes, F.; Manthe, U. A Multi-Configurational Time-Dependent Hartree Approach to the Direct Calculation of Thermal Rate Constants. *J. Chem. Phys.* **1997**, *106*, 2646–2653.
- (159) Jiang, B.; Guo, H. Relative Efficacy of Vibrational vs. Translational Excitation in Promoting Atom-Diatom Reactivity: Rigorous Examination of Polanyi's Rules and Proposition of Sudden Vector Projection (SVP) Model. *J. Chem. Phys.* **2013**, *138*, 234104.
- (160) Jiang, B.; Guo, H. Control of Mode/Bond Selectivity and Product Energy Disposal by the Transition State: The X + H<sub>2</sub>O (X=H, F, O(<sup>3</sup>P), and Cl) Reactions. *J. Am. Chem. Soc.* **2013**, *135*, 15251–15256.
- (161) Jiang, B.; Guo, H. Mode Specificity, Bond Selectivity, and Product Energy Disposal in X + CH<sub>4</sub>/CHD<sub>3</sub> (X=H, F, O(<sup>3</sup>P), Cl, and OH) Hydrogen Abstraction Reaction: Perspective from Sudden Vector Projection Model. *J. Chin. Chem. Soc.* **2014**, *61*, 841–959.
- (162) Jiang, B.; Li, J.; Guo, H. Effects of Reactant Rotational Excitation on Reactivity: Perspectives from the Sudden Limit. *J. Chem. Phys.* **2014**, *140*, 034112.
- (163) Li, J.; Guo, H. Mode Specificity in Unimolecular Reactions, Insights from the Sudden Vector Projection Model. *J. Phys. Chem. A* **2014**, *118*, 2419–2425.
- (164) Child, M. S.; Halonen, L. Overtone Frequencies and Intensities in the Local Mode Picture. *Adv. Chem. Phys.* **1984**, *57*, 1–58.
- (165) Miller, W. H.; Handy, N. C.; Adams, J. E. Reaction Path Hamiltonian for Polyatomic Molecules. *J. Chem. Phys.* **1980**, *72*, 99–112.
- (166) Jiang, B.; Guo, H. Prediction of Mode Specificity, Bond Selectivity, Normal Scaling, and Surface Lattice Effects in Water Dissociative Chemisorption on Several Metal Surfaces Using the Sudden Vector Projection Model. *J. Phys. Chem. C* **2014**, *118*, 26851–26858.
- (167) Guo, H.; Jiang, B. The Sudden Vector Projection Model for Reactivity: Mode Specificity and Bond Selectivity Made Simple. *Acc. Chem. Res.* **2014**, *47*, 3679–3685.
- (168) Ishikawa, Y.; Nakajima, T.; Yanai, T.; Hirao, K. Ab Initio Direct Molecular Dynamics Study of the Fragmentation of F(H<sub>2</sub>O) Complex Generated by Photodetachment of F<sup>−</sup>(H<sub>2</sub>O) Anion Complex. *Chem. Phys. Lett.* **2002**, *363*, 458–464.
- (169) Deskevich, M. P.; Nesbitt, D. J.; Werner, H.-J. Dynamically Weighted Multiconfiguration Self-Consistent Field: Multistate Calculations for F + H<sub>2</sub>O → HF + OH Reaction Paths. *J. Chem. Phys.* **2004**, *120*, 7281–7289.
- (170) Li, G.; Zhou, L.; Li, Q.-S.; Xie, Y.; Schaefer, H. F., III The Entrance Complex, Transition State, and Exit Complex for the F + H<sub>2</sub>O → HF + OH Reaction. Definitive Predictions. Comparison with Popular Density Functional Methods. *Phys. Chem. Chem. Phys.* **2012**, *14*, 10891–10895.
- (171) Li, G.; Li, Q.-S.; Xie, Y.; Schaefer, H. F., III The F + (H<sub>2</sub>O)<sub>2</sub> Reaction: The Second Water Removes the Barrier. *J. Phys. Chem. A* **2013**, *117*, 11979–11982.

- (172) Czakó, G.; Császár, A. G.; Schaefer, H. F. Surprising Quenching of the Spin–Orbit Interaction Significantly Diminishes  $\text{H}_2\text{O}\cdots\text{X}$  [X = F, Cl, Br, I] Dissociation Energies. *J. Phys. Chem. A* **2014**, *118*, 11956–11961.
- (173) Li, J.; Dawes, R.; Guo, H. An Ab Initio Based Full-Dimensional Global Potential Energy Surface for  $\text{FH}_2\text{O}(\text{X}^2\text{A}')$  and Dynamics for the  $\text{F} + \text{H}_2\text{O} \rightarrow \text{HF} + \text{HO}$  Reaction. *J. Chem. Phys.* **2012**, *137*, 094304.
- (174) Li, J.; Jiang, B.; Guo, H. Spin-Orbit Corrected Full-Dimensional Potential Energy Surfaces for the Two Lowest-Lying Electronic States of  $\text{FH}_2\text{O}$  and Dynamics for the  $\text{F} + \text{H}_2\text{O} \rightarrow \text{HF} + \text{OH}$  Reaction. *J. Chem. Phys.* **2013**, *138*, 074309.
- (175) Li, J.; Li, Y.; Guo, H. Communication. Covalent Nature of the  $\text{X}\cdots\text{H}_2\text{O}$  (X=F, Cl, Br) Interactions. *J. Chem. Phys.* **2013**, *138*, 141102.
- (176) Nguyen, T. L.; Li, J.; Dawes, R.; Stanton, J. F.; Guo, H. Accurate Determination of Barrier Height and Kinetics for the  $\text{F} + \text{H}_2\text{O} \rightarrow \text{HF} + \text{OH}$  Reaction. *J. Phys. Chem. A* **2013**, *117*, 8864–8872.
- (177) Li, J.; Guo, H. Quasi-Classical Trajectory Study of the  $\text{F} + \text{H}_2\text{O} \rightarrow \text{HF} + \text{OH}$  Reaction: Influence of Barrier Height, Reactant Rotational Excitation, and Isotopic Substitution. *Chin. J. Chem. Phys.* **2013**, *26*, 627–634.
- (178) Li, J.; Jiang, B.; Guo, H. Enhancement of Bimolecular Reactivity by a Pre-Reaction Van Der Waals Complex: The Case of  $\text{F} + \text{H}_2\text{O} \rightarrow \text{HF} + \text{HO}$ . *Chem. Sci.* **2013**, *4*, 629–632.
- (179) Skouteris, D.; Manolopoulos, D. E.; Bian, W.; Werner, H.-J.; Lai, L.-H.; Liu, K. Van Der Waals Interactions in the  $\text{Cl} + \text{HD}$  Reaction. *Science* **1999**, *286*, 1713–1716.
- (180) Czakó, G.; Bowman, J. M. CH Stretching Excitation Steers the F Atom to the CD Bond in the  $\text{F} + \text{CHD}_3$  Reaction. *J. Am. Chem. Soc.* **2009**, *131*, 17534–17535.
- (181) Czakó, G.; Bowman, J. M. Dynamics of the Reaction of Methane with Chlorine Atom on a Accurate Potential Energy Surface. *Science* **2011**, *334*, 343–346.
- (182) Li, J.; Jiang, B.; Guo, H. Reactant Vibrational Excitations of Reactant are More Effective Than Translational Energy in Promoting an Early-Barrier Reaction  $\text{F} + \text{H}_2\text{O} \rightarrow \text{HF} + \text{OH}$ . *J. Am. Chem. Soc.* **2013**, *135*, 982–985.
- (183) Song, H.; Li, J.; Guo, H. Mode Specificity in the  $\text{HF} + \text{OH} \rightarrow \text{F} + \text{H}_2\text{O}$  Reaction. *J. Chem. Phys.* **2014**, *141*, 164316.
- (184) Li, J.; Corchado, J. C.; Espinosa-García, J.; Guo, H. Final State-Resolved Mode Specificity in  $\text{HX} + \text{OH} \rightarrow \text{X} + \text{H}_2\text{O}$  (X=F and Cl) Reactions: A Quasi-Classical Trajectory Study. *J. Chem. Phys.* **2015**, *142*, 084314.
- (185) Song, H.; Guo, H. Mode Specificity in Bond Selective Reactions  $\text{F} + \text{HOD} \rightarrow \text{HF} + \text{OD}$  and  $\text{DF} + \text{OH}$ . *J. Chem. Phys.* **2015**, *142*, 174309.
- (186) Nyman, G.; Clary, D. C. Vibrational and Rotational Effects in the  $\text{Cl} + \text{HOD} \rightarrow \text{HCl} + \text{OD}$  Reaction. *J. Chem. Phys.* **1994**, *100*, 3556–3567.
- (187) Clary, D. C.; Nyman, G.; Hernandez, R. Mode Selective Chemistry in the Reactions of OH with HBr and HCl. *J. Chem. Phys.* **1994**, *101*, 3704–3714.
- (188) Yu, H. G.; Nyman, G. Interpolated Ab Initio Quantum Scattering for the Reaction of OH with HCl. *J. Chem. Phys.* **2000**, *113*, 8936–8944.
- (189) Rodriguez, A.; Garcia, E.; Hernandez, M. L.; Laganà, A. A LAGROBO Strategy to Fit Potential Energy Surfaces: The OH + HCl Reaction. *Chem. Phys. Lett.* **2002**, *360*, 304–312.
- (190) Garcia, E.; Rodriguez, A.; Hernandez, M. L.; Lagana, A. A LAGROBO Multiproperty Fit to Four-Atom Potential Energy Surfaces: The OH + HCl Case Study. *J. Phys. Chem. A* **2003**, *107*, 7248–7257.
- (191) Wormer, P. E. S.; Klos, J. A.; Groenenboom, G. C.; van der Avoird, A. Ab Initio Computed Diabatic Potential Energy Surfaces of OH-HCl. *J. Chem. Phys.* **2005**, *122*, 244325.
- (192) Rodriguez, A.; Garcia, E.; Luz Hernandez, M.; Laganà, A. Isotopic Effects in the Product Vibrational Distribution of the  $\text{OH}(\text{OD}) + \text{HCl}$  Reaction. *Chem. Phys. Lett.* **2003**, *371*, 223–228.
- (193) Rougeau, N.; Nyman, G.; Kubach, C. Quantum Studies of  $\text{H}_2\text{O} + \text{Cl} \rightarrow \text{HO} + \text{HCl}$  and  $\text{H}_2\text{O} + \text{Br} \rightarrow \text{HO} + \text{HBr}$  Reactions. A Comparison of Two Reduced Dimensionality Approaches. *Phys. Chem. Chem. Phys.* **1999**, *1*, 1191–1196.
- (194) Fair, J. R.; Schaefer, D.; Kosloff, R.; Nesbitt, D. J. Intramolecular Energy Flow and Nonadiabaticity in Vibrational Mediated Chemistry: Wave Packet Studies of  $\text{Cl} + \text{H}_2\text{O}$ . *J. Chem. Phys.* **2002**, *116*, 1406–1416.
- (195) Huarte-Larrañaga, F.; Manthe, U. Quantum Mechanical Calculation of the  $\text{OH} + \text{HCl} \rightarrow \text{H}_2\text{O} + \text{Cl}$  Reaction Rate: Full Dimensional Accurate, Centrifugal Sudden, and J-Shifted Results. *J. Chem. Phys.* **2003**, *118*, 8261–8267.
- (196) Rougeau, N. Planar Study of  $\text{H}_2\text{O} + \text{Cl} \leftrightarrow \text{HO} + \text{HCl}$  Reactions. *Phys. Chem. Chem. Phys.* **2007**, *9*, 2113–2120.
- (197) Li, J.; Dawes, R.; Guo, H. Kinetic and Dynamic Studies of the  $\text{Cl}({}^2\text{P}_u) + \text{H}_2\text{O}({}^1\text{A}_1) \rightarrow \text{HCl}({}^1\text{S}^+) + \text{OH}({}^2\text{P}^-)$  Reaction on an Ab Initio Based Full-Dimensional Global Potential Energy Surface of the Ground Electronic State of  $\text{ClH}_2\text{O}$ . *J. Chem. Phys.* **2013**, *139*, 074302.
- (198) Guo, Y.; Zhang, M.; Xie, Y.; Schaefer, H. F., III Communication: Some Critical Features of the Potential Energy Surface for the  $\text{Cl} + \text{H}_2\text{O} \rightarrow \text{HCl} + \text{OH}$  Forward and Reverse Reactions. *J. Chem. Phys.* **2013**, *139*, 041101.
- (199) Li, J.; Song, H.; Guo, H. Insights into the Bond-Selective Reaction of  $\text{Cl} + \text{HOD}(\text{n}_{\text{OH}}) \rightarrow \text{HCl} + \text{OD}$ . *Phys. Chem. Chem. Phys.* **2015**, *17*, 4259–4267.
- (200) Song, H.; Guo, H. Mode Specificity in the  $\text{HCl} + \text{OH} \rightarrow \text{Cl} + \text{H}_2\text{O}$  Reaction: Polanyi's Rules Vs. Sudden Vector Projection Model. *J. Phys. Chem. A* **2015**, *119*, 826–831.
- (201) Guo, H. Quantum Dynamics of Complex-Forming Bimolecular Reactions. *Int. Rev. Phys. Chem.* **2012**, *31*, 1–68.
- (202) Karkach, S. P.; Oshorov, V. I. Ab Initio Analysis of the Transition States on the Lowest Triplet  $\text{H}_2\text{O}_2$  Potential Surface. *J. Chem. Phys.* **1999**, *110*, 11918–11927.
- (203) Harding, L. B.; Wagner, A. F. Theoretical Study of the Reaction Rates of  $\text{OH} + \text{OH} \rightleftharpoons \text{H}_2\text{O} + \text{O}$ . *Symp. (Int.) Combust., [Proc.]* **1989**, *22*, 983–989.
- (204) Nguyen, T. L.; Stanton, J. F. Ab Initio Thermal Rate Calculations of  $\text{HO} + \text{HO} = \text{O}({}^3\text{P}) + \text{H}_2\text{O}$  Reaction and Isotopologues. *J. Phys. Chem. A* **2013**, *117*, 2678–2686.
- (205) Braunstein, M.; Panfili, R.; Shroll, P.; Bernstein, L. Potential Surfaces and Dynamics of the  $\text{O}({}^3\text{P}) + \text{H}_2\text{O}({}^1\text{A}_1) \rightarrow \text{OH}({}^2\text{P}^-)$  Reaction. *J. Chem. Phys.* **2005**, *122*, 184307.
- (206) Conforti, P. F.; Braunstein, M.; Braams, B. J.; Bowman, J. M. Global Potential Energy Surfaces for  $\text{O}({}^3\text{P}) + \text{H}_2\text{O}({}^1\text{A}_1)$  Collisions. *J. Chem. Phys.* **2010**, *133*, 164312.
- (207) Braunstein, M.; Conforti, P. F. O-Atom Exchange in  $\text{O}({}^3\text{P}) + \text{H}_2\text{O}({}^1\text{A}_1)$  Collisions. *Chem. Phys. Lett.* **2012**, *523*, 34–38.
- (208) Braunstein, M.; Conforti, P. F. Classical Dynamics of State-Resolved Hyperthermal  $\text{O}({}^3\text{P}) + \text{H}_2\text{O}({}^1\text{A}_1)$  Collisions. *J. Chem. Phys.* **2013**, *138*, 074303.
- (209) Li, J.; Guo, H. A New Ab Initio Based Global  $\text{HOOH}({}^1\text{A}''')$  Potential Energy Surface for the  $\text{O}({}^3\text{P}) + \text{H}_2\text{O}({}^1\text{A}_1) \leftrightarrow \text{OH}({}^2\text{P}^-) + \text{OH}({}^2\text{P}^-)$  Reaction. *J. Chem. Phys.* **2013**, *138*, 194304.
- (210) de Oliveira-Filho, A. G. S.; Ornella, F. R.; Bowman, J. M. Quasiclassical Trajectory Calculations of the Rate Constant of the  $\text{OH} + \text{HBr} \rightarrow \text{Br} + \text{H}_2\text{O}$  Reaction Using a Full-Dimensional Ab Initio Potential Energy Surface over the Temperature Range 5 to 500 K. *J. Phys. Chem. Lett.* **2014**, *5*, 706–712.
- (211) Zhang, M.; Hao, Y.; Guo, Y.; Xie, Y.; Schaefer, H. Anchoring the Potential Energy Surface for the  $\text{Br} + \text{H}_2\text{O} \rightarrow \text{HBr} + \text{OH}$  Reaction. *Theor. Chem. Acc.* **2014**, *133*, 1–9.
- (212) Hao, Y.; Gu, J.; Guo, Y.; Zhang, M.; Xie, Y.; Schaefer, H. F., III Spin-Orbit Corrected Potential Energy Surface Features for the  $\text{I}({}^2\text{P}_{3/2}) + \text{H}_2\text{O} \rightarrow \text{HI} + \text{OH}$  Forward and Reverse Reactions. *Phys. Chem. Chem. Phys.* **2014**, *16*, 2641–2646.
- (213) Clary, D. C.; Stoecklin, T. S.; Wickham, A. G. Rate Constants for Chemical Reactions of Radicals at Low Temperatures. *J. Chem. Soc., Faraday Trans.* **1993**, *89*, 2185–2191.
- (214) Nizamov, B.; Setser, D. W.; Wang, H.; Peslherbe, G. H.; Hase, W. L. Quasiclassical Trajectory Calculations for the  $\text{OH}({}^2\text{P}^-)$  and  $\text{OD}({}^2\text{P}^-) + \text{HBr}$  Reactions: Energy Partitioning and Rate Constants. *J. Chem. Phys.* **1996**, *105*, 9897–9911.
- (215) Liu, J.-y.; Li, Z.-s.; Dai, Z.-w.; Huang, X.-r.; Sun, C.-c. Direct Ab Initio Dynamics Calculations of the Reaction Rates for the Hydrogen

Abstraction OH + HBr → H<sub>2</sub>O + Br. *J. Phys. Chem. A* **2001**, *105*, 7707–7712.

(216) de Oliveira-Filho, A. G. S.; Ornellas, F. R.; Bowman, J. M. Energy Disposal and Thermal Rate Constants for the OH + HBr and OH + DBr Reactions: Quasiclassical Trajectory Calculations on an Accurate Potential Energy Surface. *J. Phys. Chem. A* **2014**, *118*, 12080–12088.

(217) Che, D.-C.; Matsuo, T.; Yano, Y.; Bonnet, L.; Kasai, T. Negative Collision Energy Dependence of Br Formation in the OH + HBr Reaction. *Phys. Chem. Chem. Phys.* **2008**, *10*, 1419–1423.

(218) Jiang, B.; Guo, H. Mode and Bond Selectivities in Methane Dissociative Chemisorption: Quasi-Classical Trajectory Studies on Twelve-Dimensional Potential Energy Surface. *J. Phys. Chem. C* **2013**, *117*, 16127–16135.

(219) Jiang, B.; Liu, R.; Li, J.; Xie, D.; Yang, M.; Guo, H. Mode Selectivity in Methane Dissociative Chemisorption on Ni(111). *Chem. Sci.* **2013**, *4*, 3249–3254.

(220) Jiang, B.; Guo, H. Six-Dimensional Quantum Dynamics for Dissociative Chemisorption of H<sub>2</sub> and D<sub>2</sub> on Ag(111) on a Permutation Invariant Potential Energy Surface. *Phys. Chem. Chem. Phys.* **2014**, *16*, 24704–24715.

(221) Jackson, B.; Nattino, F.; Kroes, G.-J. Dissociative Chemisorption of Methane on Metal Surfaces: Tests of Dynamical Assumptions Using Quantum Models and Ab Initio Molecular Dynamics. *J. Chem. Phys.* **2014**, *141*, 054102.

(222) Hundt, P. M.; Jiang, B.; van Reijzen, M.; Guo, H.; Beck, R. D. vibrationally Promoted Dissociation of Water on Ni(111). *Science* **2014**, *344*, 504–507.

(223) Jiang, B.; Guo, H. Dynamics of Water Dissociative Chemisorption on Ni(111): Effects of Impact Sites and Incident Angles. *Phys. Rev. Lett.* **2015**, *114*, 166101.

(224) Li, A.; Guo, H. A Nine-Dimensional Ab Initio Global Potential Energy Surface for the H<sub>2</sub>O<sup>+</sup> + H<sub>2</sub> → H<sub>3</sub>O<sup>+</sup> + H Reaction. *J. Chem. Phys.* **2014**, *140*, 224313.

(225) Li, J.; Guo, H. A Nine-Dimensional Global Potential Energy Surface for NH<sub>4</sub>(X<sup>2</sup>A<sub>1</sub>) and Kinetics Studies on the H + NH<sub>3</sub> ↔ H<sub>2</sub> + NH<sub>2</sub> Reaction. *Phys. Chem. Chem. Phys.* **2014**, *16*, 6753–6763.

(226) Song, H.; Li, J.; Yang, M.; Lu, Y.; Guo, H. Nine-Dimensional Quantum Dynamics Study of the H<sub>2</sub> + NH<sub>2</sub> → H + NH<sub>3</sub> Reaction: A Rigorous Test of the Sudden Vector Projection Model. *Phys. Chem. Chem. Phys.* **2014**, *16*, 17770–17776.